Cellular/Molecular

Synaptotagmin-11 Inhibits Synaptic Vesicle Endocytosis via Endophilin A1

Yalong Wang,[1,2*] Ying Zhu,[3,4*] Wanru Li,[2] Shuxin Yan,[2] Chao Li,[3,4,5] Kunpeng Ma,[1] Meiqin Hu,[6] Cuilian Du,[2] Lei Fu,[7] Jianyuan Sun,[1,2,3,4] and Claire Xi Zhang[2,7]

[1]Brain Cognition and Brain Disease Institute, Shenzhen Institute of Advanced Technology, Chinese Academy of Sciences; CAS Key Laboratory of Brain Connectome and Manipulation; Shenzhen-Hong Kong Institute of Brain Science-Shenzhen Fundamental Research Institutions, Shenzhen, Guangdong 518055, China, [2]Beijing Institute of Brain Disorders, Laboratory of Brain Disorders, Ministry of Science and Technology, Collaborative Innovation Center for Brain Disorders, Capital Medical University, Beijing, 100069, China, [3]State Key Laboratory of Brain and Cognitive Sciences, Institute of Biophysics, Chinese Academy of Sciences, Beijing, 100101, China, [4]University of Chinese Academy of Sciences, Beijing, 100049, China, [5]Key Laboratory of RNA Biology, Institute of Biophysics, Chinese Academy of Sciences, Beijing, 100101, China, [6]Department of Molecular, Cellular, and Developmental Biology, University of Michigan, Ann Arbor, Michigan 48109, and [7]Academy of Pharmacy, Xi'an Jiaotong-Liverpool University, Suzhou, Jiangsu 215123, China

Synaptic vesicle (SV) endocytosis is a critical and well-regulated process for the maintenance of neurotransmission. We previously reported that synaptotagmin-11 (Syt11), an essential non-Ca^{2+}-binding Syt associated with brain diseases, inhibits neuronal endocytosis (Wang et al., 2016). Here, we found that Syt11 deficiency caused accelerated SV endocytosis and vesicle recycling under sustained stimulation and led to the abnormal membrane partition of synaptic proteins in mouse hippocampal boutons of either sex. Furthermore, our study revealed that Syt11 has direct but Ca^{2+}-independent binding with endophilin A1 (EndoA1), a membrane curvature sensor and endocytic protein recruiter, with high affinity. EndoA1-knockdown significantly reversed Syt11-KO phenotype, identifying EndoA1 as a main inhibitory target of Syt11 during SV endocytosis. The N-terminus of EndoA1 and the C2B domain of Syt11 were responsible for this interaction. A peptide (amino acids 314-336) derived from the Syt11 C2B efficiently blocked Syt11–EndoA1 binding both *in vitro* and *in vivo*. Application of this peptide inhibited SV endocytosis in WT hippocampal neurons but not in EndoA1-knockdown neurons. Moreover, intracellular application of this peptide in mouse calyx of Held terminals of either sex effectively hampered both fast and slow SV endocytosis at physiological temperature. We thus propose that Syt11 ensures the precision of protein retrieval during SV endocytosis by inhibiting EndoA1 function at neuronal terminals.

Key words: **endophilin; synaptic vesicle; endocytosis; synaptotagmin**

Significance Statement

Endocytosis is a key stage of synaptic vesicle (SV) recycling. SV endocytosis retrieves vesicular membrane and protein components precisely to support sustained neurotransmission. However, the molecular mechanisms underlying the regulation of SV endocytosis remain elusive. Here, we reported that Syt11-KO accelerated SV endocytosis and impaired membrane partition of synaptic proteins. EndoA1 was identified as a main inhibitory target of Syt11 during SV endocytosis. Our study reveals a novel inhibitory mechanism of SV endocytosis in preventing hyperactivation of endocytosis, potentially safeguarding the recycling of synaptic proteins during sustained neurotransmission.

Received June 29, 2021; revised May 12, 2023; accepted June 2, 2023.

Author contributions: Y.W., J.S., and C.X.Z. designed research; Y.W., Y.Z., W.L., S.Y., and M.H. performed research; Y.W., Y.Z., C.L., K.M., and C.D. analyzed data; Y.W., Y.Z., J.S., and C.X.Z. wrote the first draft of the paper; C.L., K.M., and L.F. contributed unpublished reagents/analytic tools; L.F., J.S., and C.X.Z. edited the paper; L.F., J.S., and C.X.Z. wrote the paper.

This study was supported by National Natural Science Foundation of China 31471085 to C.X.Z., and U20A6005 and 31527802 to J.S.; SIP High-Quality Innovation Platform for Chronic Diseases YZCXPT2022203 to L.F. and C.X.Z.; National Basic Research Program of China 2013CB835100 to J.S.; Instrument Development Project CAS YJKYYQ20180028 to J.S.; Key Research Program of Frontier Sciences CAS QYZDYSSW-SMC015 to J.S.; STI2030-Major Projects 2021ZD0202500 to J.S.; Shenzhen Infrastructure for Brain Analysis and Modeling 202100105 to J.S.; and China Postdoctoral Science Foundation 2021M693297 to Y.W. We thank Prof. Xiaomin Wang and Dr. Lin Dong for valuable suggestions and technical support.

*Y.W. and Y.Z. contributed equally to this work.

The authors declare no competing financial interests.

Correspondence should be addressed to Jianyuan Sun at jy.sun1@siat.ac.cn or Claire Xi Zhang at Xi.Zhang@xjtlu.edu.cn.

https://doi.org/10.1523/JNEUROSCI.1348-21.2023

Introduction

In synapses, sustained neurotransmission demands robust synaptic vesicle (SV) exocytosis, which is supported by active and precise vesicle recycling (Saheki and De Camilli, 2012). Terminals develop complex endocytosis mechanisms to maintain the integrity of synaptic structures, clear the release sites, and ensure the replenishment of vesicle pools (Wu et al., 2014; Lou, 2018). Multiple endocytic modes, such as clathrin-mediated endocytosis (CME), bulk endocytosis, "kiss-and-run", and fast and ultrafast endocytosis, have been proposed to retrieve the components of SVs, including membranes and proteins from synaptic membrane in a synapse-specific manner (Smith et al., 2008; Soykan et al., 2016; Watanabe and Boucrot, 2017; Milosevic, 2018). In addition, different synaptic proteins use distinct sorting pathways (Koo et al., 2011, 2015; Kononenko et al., 2013; Kaempf et al., 2015) and vesicle size is well controlled (Zhang et al., 1998; Shimizu et al., 2003). SV endocytosis is also tightly regulated by both positive and negative regulators. Many regulators have been reported to facilitate SV endocytosis, including Ca^{2+} (Yamashita, 2012; Leitz and Kavalali, 2016), calmodulin (Wu et al., 2009), calcineurin (Wu et al., 2014), Syt1 (Poskanzer et al., 2003; Yao et al., 2012; Li et al., 2017), SNARE proteins (Deak et al., 2004; Diao et al., 2013; Xu et al., 2013), and flower (Yao et al., 2009), while inhibitory mechanisms have rarely been revealed (Smith et al., 2008; Leitz and Kavalali, 2016; Wang and Zhang, 2017). We previously discovered that Syt11 inhibits multiple endocytic pathways in neurons and hypothesized that it functions to safeguard the precision of endocytosis (Wang et al. 2016). However, some pieces of evidence for this hypothesis are yet to be revealed and the molecular mechanism underlying Syt11 inhibition is unknown.

Syt11 is associated with schizophrenia (Inoue et al., 2007) and Parkinson's disease (Huynh et al., 2003; Glass et al., 2004; Pihlstrom et al., 2013; Bento et al., 2016; Sesar et al., 2016; Wang et al., 2018) and is essential for development and synaptic plasticity (Shimojo et al., 2019). Syt11 mRNA (Mittelsteadt et al., 2009) and protein (Shimojo et al., 2019) are abundant in most brain areas. It is composed of a short luminal N-terminus, a transmembrane domain, and a linker region followed by two evolutionarily conserved cytoplasmic domains (C2A and C2B). A permutation in Syt11-C2A at position 247 from aspartate to serine abolishes its Ca^{2+}-dependent phospholipid binding (von Poser et al., 1997). We reported that in Syt11-knockdown (KD) DRG neurons, both CME and bulk endocytosis accelerate, with increased endocytic sites on the plasma membrane (Wang et al., 2016). The endocytosed vesicle size remains unaffected. In the KD terminals of hippocampal neurons, SV endocytosis revealed by FM4-64 uptake and discharge is also enhanced, but the kinetics of stimulus-coupled exocytosis is unchanged. *In vivo* experiments have shown that overexpression of Syt11 in the substantia nigra pars compacta impairs ipsilateral striatal dopamine release by inhibiting endocytosis, leading to the degeneration of dopaminergic neurons and progressive contralateral motor abnormalities (Wang et al., 2018). Here we show that Syt11 functions in SV endocytosis and assess its impact on the partition of synaptic proteins. We identify EndoA1 as a protein directly interacting with Syt11. The physiological function of the Syt11–EndoA1 interaction is demonstrated by an inhibitory effect on SV endocytosis in both hippocampal and calyx of Held terminals through a competing peptide derived from the C2B domain of Syt11.

Materials and Methods

Animals. The floxed Syt11 knock-in mice were purchased from The Jackson Laboratory (stock #008294 and strain name *B6;129-Syt11tm1^{Sdu}/J*). The generation of this mouse strain was reported by Shimojo et al. (2019). Genotyping for this strain was performed by PCR with the specific oligonucleotide primers 5′-AATCTCA GCACTCAGGAGTCAG-3′ (forward) and 5′-CTCTTGCTTACT GATTGGCAGC-3′ (reverse).

This study was performed in strict accordance with the recommendations in the *Guide for the care and use of laboratory animals* of the National Institutes of Health. All the animal experimental procedures were approved by the Ethics Committee on Animal Care and Use of Capital Medical University.

Plasmids. Rat synaptotagmin-11 (AF000423) without the N terminus and transmembrane domain (37-428) was subcloned into the pGEX4T2 vector for GST-Syt11 protein purification. Other truncated forms of Syt11, linker (37-156), Δlinker (157-428), C2A (157-290), ΔC2A (37-156 and 291-428), C2B (291-428), and ΔC2B (37-290), and the C2B mutations [GST-PP1-3 (291-359), GST-PP4-6 (360-428), GST-PP3-6 (336-428), GST-PP2-6 (314-428), and GST-PP1-2 (291-335)] used the same vector. The 6xHis tag was added to the N-terminus of full-length EndoA1 (1-352), Δ Src homology 3 (SH3) (1-293 and 348-352), and SH3 (293-347) separately, which were subcloned into the pET28a vector for His-tagged protein expression and purification.

Three-myc tagged full-length Syt11 (AF000423) was subcloned into pcDNA3.1. GFP-EndoA1, Syb2-pHluorin, and Syt1-pHluorin were kind gifts from Prof. Peter S McPherson, Prof. James E. Rothman, and Prof. Gero Miesenbock. The plasmids for mouse endophilin A1 silencing were constructed by inserting 5′-GCTCGATGATGACTTCAAA-3′ (shRNA1) and 5′-GGGCTAAGCTCAGTATGAT-3′ (shRNA2) into the pLKD-CMV-eGFP-U6-shRNA vector, while the nontargeting sequence 5′-TTCTCCGAACGTGTCACGT-3′ served as a control. All the constructs were confirmed by DNA sequencing.

Antibodies and chemicals. The primary antibodies used for Western blotting were anti-synaptotagmin 11 (270003, Synaptic Systems), anti-clathrin heavy chain (610499, BD Transduction Laboratories), anti-AP2 α-adaptin (610501, BD Transduction Laboratories), anti-dynamin 1 (2441931, Millipore), anti-caveolin 1 (N-20) (sc-894, Santa Cruz Biotechnology), anti-synapsin 1 (106011, Synaptic Systems), anti-synaptotagmin 1 (105103, Synaptic Systems), anti-synaptophysin 1 (101011, Synaptic Systems), anti-synaptobrevin (104211, Synaptic Systems), anti-α-synuclein (610787, BD Transduction Laboratories), anti-β-actin (A1978, Sigma), anti–voltage-dependent anion channel (4866, Cell Signaling), anti-GAPDH (G8795, Sigma), anti-transferrin receptor (TfR, ab84036, Abcam), anti-TGN46 (ab16059, Abcam), anti-Na^+/K^+-ATPase α1 antibody (C464.6) (sc-21 712, Santa Cruz Biotechnology), anti-SNAP25 (111011, Synaptic Systems), anti-endophilin (D-3) (sc-48378, Santa Cruz Biotechnology), and anti-c-Myc (sc-789 and sc-40, Santa Cruz Biotechnology).

The antibodies for immunofluorescence were anti-dynamin 1 (2441931, Millipore), anti-synapsin 1 (106011, Synaptic Systems), anti-synaptobrevin 2 (104211, Synaptic Systems), anti-c-Myc (sc-789 and sc-40, Santa Cruz Biotechnology; 2272S, CST), and anti-EndoA1 (65169S, CST).

The antibodies for immunoprecipitation assays were mouse normal IgG (12-371, Millipore), rabbit normal IgG (12-370, Millipore), anti-GFP (598, MBL), anti-c-Myc (sc-789 and sc-40, Santa Cruz Biotechnology; 2272S, CST), and anti-endophilin A1 (G-8) (sc-46 702, Santa Cruz Biotechnology).

All chemicals were from Sigma unless otherwise noted.

Primary hippocampal neuron culture and plasmid transfection. Primary cultured hippocampal neurons were prepared from newborn mice of either sex within 24 h of experiments. The cells were plated on poly-D-lysine-coated 24-well plates for immunofluorescence or 25 mm coverslips for live-cell imaging. Cells were plated with DMEM containing 10% FBS for 4 h, and then the medium was switched to Neurobasal-A supplemented with 2% B-27, 0.5 mM L-glutamax, and 1% v/v penicillin/streptomycin. The neurons were transfected on DIV5 using Lipofectamine 2000 according to the manufacturer's

instructions with minor modifications. Half of the volume of culture medium was removed and saved. One microliter of Lipofectamine 2000 in 25 μl of Neurobasal-A and 1 μg of DNA in 25 μl of Neurobasal-A were incubated separately for 5 min, then mixed and incubated for 30 min at room temperature. This mixture was added to the cells. After 4 h incubation at 37°C under 5% CO_2, the medium was replaced with the previously saved medium and an equal volume of fresh medium. For FM4-64 and pHluorin experiments, the cells were transfected with 5 μl of Lipofectamine 2000 in 125 μl of Neurobasal-A and 4 μg of DNA in 125 μl of Neurobasal-A in 6-well plates.

Immunofluorescence and confocal imaging. Myc-Syt11-IRES2-BFP plasmid was transfected into hippocampal neurons for colocalization analysis as no specific commercial antibody for Syt11 immunocytochemistry is available. The overexpression level of myc-Syt11 was estimated by a lentivirus-mediated expression system and a ~70% increase over the endogenous level was detected. Neurons at DIV12 were washed once with cytobuffer (in mM as follows: 50 MES, pH 6.1, 5 $MgCl_2$, 3 EGTA, 5 glucose), and then fixed in freshly prepared 4% PFA for 40 min at room temperature. To quench any auto-fluorescence, the cells were washed twice for 10 min each with 1 mg/ml $NaBH_4$ in TBS (in mM as follows: 20 Tris, pH 7.5, 154 NaCl, 2 EGTA, 2 $MgCl_2$). The cells were then permeabilized and blocked with TBS containing 2% BSA and 0.02% saponin (0.5 ml/well) for 1.5 h. After incubation with primary antibodies overnight at 4°C, the cells were washed 3 times with TBS, and then incubated for 1 h with secondary antibodies. After three washes with TBS, the cells were mounted on slides with mounting medium containing 50% DAPI. The cells were scanned under a Leica TCS SP8 confocal microscope with a 63× objective and 2.5× digital zoom. The colocalization images were analyzed using the Pearson's coefficient plug-in in NIH ImageJ software.

Lentivirus infection, live-cell imaging, and image analysis. Lentiviruses for Syt11 KO were prepared by transfecting HEK293T cells with the pFUGW plasmid, which encodes the EGFP followed by a nuclear localization signal (NLS) and cre recombinase sequence (EGFP-NLS-CRE), and three helper plasmids (pRev, pRRE, and pVSVG) (a kind gift from Prof. Chen Zhang of Capital Medical University). For lentivirus packaging, plasmids of cre/Δcre/shRNA for EndoA1 (12 μg), RRE (4 μg), Rev (4 μg), and VsVg (4 μg) were mixed well; and 900 μl opti-MEM and 48 μl PEI (1 μg/μl) were added. The mixture was incubated at room temperature for 30 min, and transferred drop-wise to HEK293T cells in a 10 cm dish. After 24 h, the medium was replaced with 10 ml neuron growth medium; and after another 48 h, lentivirus was collected in the supernatant by spinning the medium at 3000 × *g* for 5 min. For neuronal cultures in 6-well plates, 300 μl virus per well was added to neurons at DIV4-DIV5. The neurons were further cultured for at least 7 d before use.

To record FM4-64 uptake and discharge, neurons at DIV12-DIV14 were washed in 1 ml cytobuffer (in mM as follows: 150 NaCl, 5 KCl, 2.5 $CaCl_2{\cdot}2H_2O$, 1 $MgCl_2{\cdot}6H_2O$, 10 HEPES, pH 7.4, 10 glucose), and incubated with 20 μM FM4-64 and 100 mM K^+ for various times at 37°C. The cells were washed 3 times in cytobuffer for 60 s each to remove free dye. Before imaging, the cells were bathed in prewarmed cytobuffer containing 50 μM AP-5 and 10 μM CNQX to block glutamate signaling during stimulation. The FM4-64 signal was recorded by spinning disk confocal microscopy (Olympus, IX83) through a 60× oil-immersion lens. To unload the FM4-64 dye, we used 800 action potentials (APs) at 40 Hz. The fluorescence changes at each bouton were visualized at 514 nm excitation and 694 nm emission. Image acquisition started 20 s before stimulation at 1 s intervals and lasted for 80 s.

For the pHluorin kinetics recording, Syt1/Syb2-pHluorin transfected neurons at DIV14 were bathed in cytobuffer (in mM as follows: 150 NaCl, 5 KCl, 2.5 $CaCl_2{\cdot}2H_2O$, 1 $MgCl_2{\cdot}6H_2O$, 10 HEPES, pH 7.4, 10 glucose) supplied with AP-5 (50 μM) and CNQX (10 μM). Images were captured at 1 s intervals for 20 s to establish a stable baseline. Then neurons were stimulated with 500 pulses delivered at 10 Hz via two parallel platinum wires embedded in the imaging chamber. Data were analyzed with ImageJ and plotted by GraphPad Prism 5.

To estimate the cell surface fraction of Syt1/Syb2-pHluorin, neurons were cotransfected with cre/Δcre and pHluorin-tagged protein and cultured to DIV12-DIV14. The cells were first washed with 1 ml imaging buffer (in mM as follows: 136 NaCl, 2.5 KCl, 2 $CaCl_2$, 1.3 $MgCl_2$, 10 glucose, 10 HEPES, pH 7.4) and then bathed in 1 ml prewarmed imaging buffer. The surface fraction was quenched by perfusing with acidic imaging buffer (pH 5.5) for 30 s, followed by standard imaging buffer (pH 7.4) to determine the recovery ratio by SV recycling. Finally, NH_4Cl was applied for 30 s to excite the total immunofluorescence intensity of pHluorin. Ten image frames were acquired at each stage at 2 s intervals to record the immunofluorescence intensity of pHluorin proteins.

For FM or pHluorin analysis, a 2-μm-diameter ROI was drawn on presynaptic boutons, and the peak fluorescence value of individual ROI was exported to Microsoft Excel for analysis by plotting *z* axis profiles with ImageJ.

Synaptosome extraction. Synaptosomes were extracted from rat brain of either sex as in Dunkley et al. (2008). Briefly, rat cortex was isolated and lysed by a glass homogenizer. Two milliliters of different concentrations of Percoll (23%, 15%, 10%, and 3%) were layered into a centrifuge tube. The 2 ml cortical lysate (4-5 mg/ml) was laid on top of the 3% Percoll. After centrifugation (fixed angle rotor JA-20; Beckman) at 20,000 rpm for 8 min at 4°C, the proteins separated into five visible fractions (F1-F5). The same volume of each fraction was processed for Western blot (WB).

For WB, samples were run on a 10% SDS-PAGE gel and transferred to a nitrocellulose filter membrane. The membrane was blocked for 1 h with 5% nonfat dried milk (w/v) prepared in PBST (in mM as follows: 135 NaCl, 2.7 KCl, 1.5 KH_2PO_4, 8 K_2HPO_4, pH 7.2, 0.05% (v/v) Tween 20). After washing in PBST, the membrane was incubated with primary antibody in PBST containing 2% BSA at 4°C overnight. After three washes in PBST, secondary antibody was applied at room temperature for 1 h. After three washes in PBST, the membrane was scanned with an Odyssey infrared imaging system (LI-COR Biosciences).

Membrane protein preparation. Extraction of plasma membrane proteins followed the instructions in the Qproteome Plasma Membrane Protein Handbook, QIAGEN (37601). Briefly, the cells were washed with PM buffer and lysed with PL buffer. After centrifugation, the supernatant was collected to interact with PBL ligands. The bound proteins were pulled down by magnetic beads and processed for WB detection.

Immunoprecipitation. HEK293T cells cultured in 10 cm dishes were cotransfected with GFP-tagged proteins and 3×myc-tagged proteins. After 48 h of transfection, the cells were lysed with 1 ml lysis buffer (in mM as follows: 20 Tris, pH 7.5, 150 NaCl, 1 EDTA, 1 PMSF, 1x protease inhibitors, and 1% Triton X-100). Samples were sonicated on ice and rotated at 4°C for 1 h for thorough lysis. After centrifugation for 15 min at 20,000 × *g* at 4°C, the supernatant was collected and precleared for 1 h at 4°C with 20 μl 50% Protein A/G agarose beads to reduce nonspecific binding. The lysate was then incubated with 4 μg primary antibody overnight at 4°C. Fifty microliters of protein A/G agarose beads were added and incubated for 1 h at 4°C. The beads were washed 5 times in 500 μl lysis buffer, and the bound proteins were released by SDS loading buffer and processed for WB.

For immunoprecipitation with mouse brain samples, 5 mg total proteins were precleared for 1 h with 50 μl 50% Protein A/G agarose beads in 1 ml buffer. Other procedures were as described above.

Expression and purification of recombinant proteins. GST or 6×His-tag protein plasmids were transfected into BL21 cells, and protein expression was induced with 0.2 μM IPTG for 5 h at 25°C. The bacterial pellets from 200 ml culture medium were suspended with 10 ml lysis buffer (in mM as follows: 50 NaH_2PO_4, 300 NaCl, pH 8.0) containing 1 mg/ml lysozyme, 1× protease inhibitor, and 1 mM PMSF. The cells were lysed for 30 m on ice and sonicated. To extract GST proteins, the centrifuged supernatant was incubated with 200 μl glutathione Sepharose beads (17-0756-01, GE Healthcare) at 4°C for 5 h. After three washes in PBS, the GST-tagged proteins on beads were used for GST pull-down experiments. To purify His-tag proteins, the centrifuged supernatant was incubated with 1 ml His-tag purification resin at 4°C for 1 h. The lysate was transferred to an Ni column, and washed 3 times with washing buffer (in mM as follows: 50 NaH_2PO_4, 300 NaCl, 2 imidazole, pH 8.0). The bound proteins were eluted with elution buffer (in mM as follows: 50 NaH_2PO_4, 300 NaCl, 50 imidazole, pH 8.0).

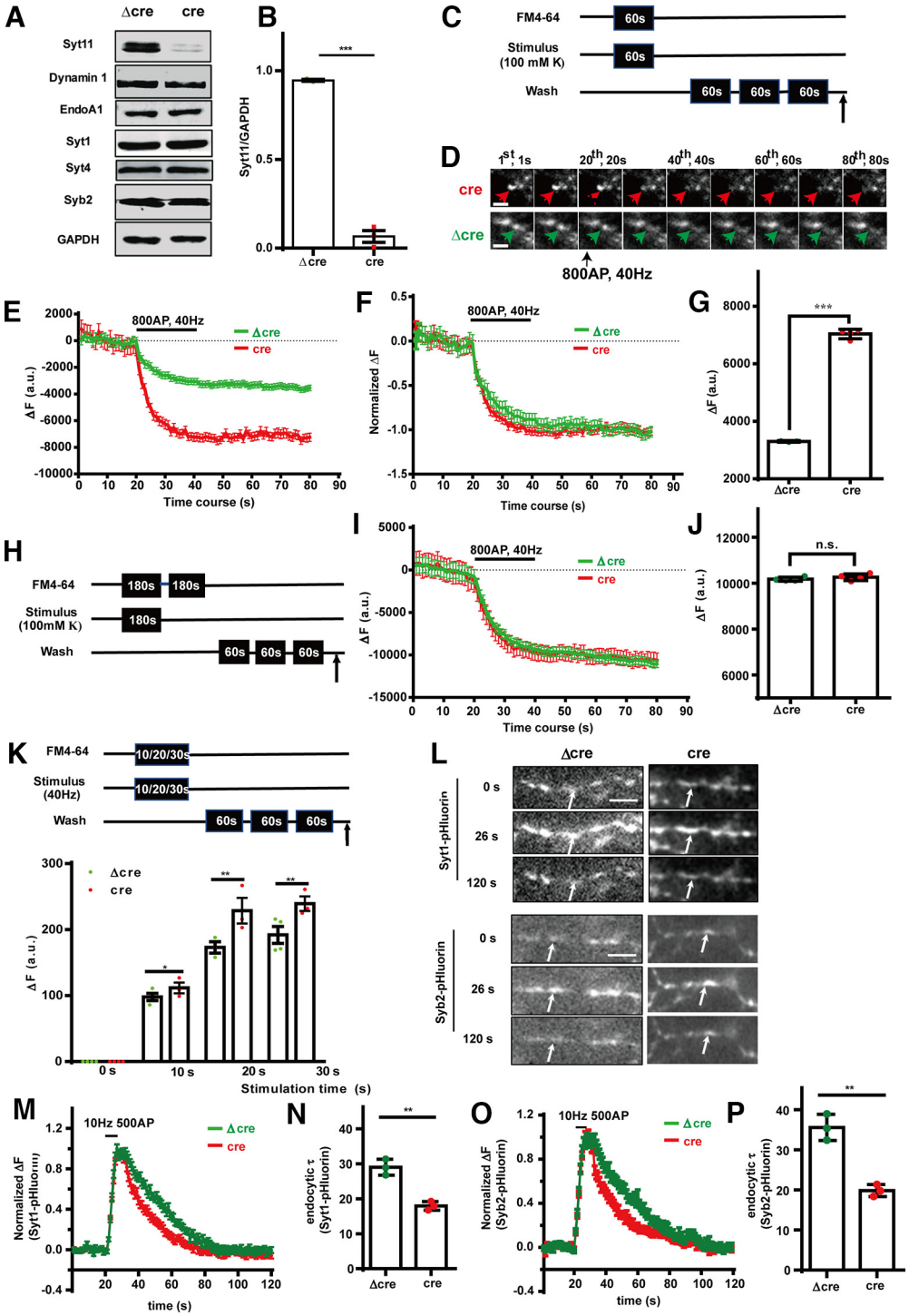

Figure 1. Syt11-KO accelerates endocytosis in hippocampal neuron terminals without affecting exocytosis. ***A***, WBs of primary cultured hippocampal neurons from floxed Syt11 knock-in mice treated with cre or Δcre-expressing lentivirus. Syt11 was efficiently knocked out, while other endocytic and synaptic proteins, such as dynamin 1, EndoA1, Syt1, Syt4, and Syb2, were unaffected. ***B***, Quantification of Syt11 protein levels as in ***A***. The KO efficiency was 94.3% from three independent experiments. $N = 3$ biological replicates. ***C***, Protocol for measuring the dischargeable FM4-64 in ***D-G***. Arrow indicates onset of image acquisition. ***D***, Representative images of FM4-64 dye loading by 100 mM K^+ and unloading by a train of 800 APs at 40 Hz. Arrows indicate exocytosis events. Scale bars, 5 μm. ***E***, Time course of FM4-64 intensity during unloading. The intensity decreased after a train of stimuli starting at 20 s. ***F***, Normalized fluorescence intensity to assess exocytosis dynamics, which was unaffected by Syt11-KO. ***G***, Quantification of normalized releasable FM4-64 dye. The releasable dye increased ~104.67% after Syt11 depletion (7038 ± 83.23 in Δcre group, 62 boutons from 4 experiments; 3302 ± 14.77 in cre group, 64 boutons from 3 experiments). ***$p < 0.001$. ***H***, Protocol for overstimulation condition. ***I***, ***J***, Averaged traces of FM4-64 unloading (800 APs at 40 Hz) after overstimulation. The FM4-64 discharge is shown as the mean ± SEM (Δcre, 10,509 ± 55.70, 73 boutons from 4 experiments; cre, 10,422 ± 41.62, 75 boutons from 4 experiments, $p = 0.21$). ***K***, FM4-64 uptake in terminals treated with cre or Δcre lentivirus. The dye was loaded with 10, 20, or 30 s of electrical stimulation at 40 Hz. Images were acquired after three washes for 1 min each. The same parameters for image acquisition were used for all groups. Numbers of analyzed boutons/coverslips are indicated. The FM4-64 uptake is presented as the mean ± SEM (10-s Δcre, 98.00 ± 1.47, 201 boutons from 3 experiments; 10-s cre, 111.70 ± 7.12, 222 boutons from 4 experiments, *$p = 0.038$; 20-s Δcre, 173.00 ± 5.33, 171 boutons from 3 experiments; 20-s cre, 228.70 ± 1.20, 192 boutons from 3 experiments, **$p = 0.0037$; 30-s Δcre, 192.00 ± 3.36, 195 boutons from 3 experiments; 30-s cre, 239.00 ± 3.78, 207 boutons from 4 experiments, **$p = 0.0084$). ***L***, Fluorescence change of Syt1-pHluorin and Syb2-pHluorin before stimulation (0 s), after stimulation (26 s), and back to baseline (120 s) in Δcre/cre group. Arrows indicate typical events of exocytosis and endocytosis. Scale bars, 5 μm. ***M–P***, Kinetic traces and endocytic τ of Syt1-

To exchange buffer, purified proteins were placed in a dialysis bag and incubated in 2 L HEKG buffer (in mM as follows: 20 HEPES, 1 EDTA, 50 KCl, pH 7.2) containing 0.4 mM PMSF at 4°C. The buffer was changed twice, every 4 h. The purified proteins were stored at –80°C.

GST pull-down. Mouse brain tissue was homogenized in lysis buffer (in mM as follows: 20 Tris, pH 7.5, 150 NaCl, 1 EDTA, 1 PMSF, 1x protease inhibitors, and 1% Triton X-100) and rotated at 4°C for 2 h. After centrifugation for 15 min at 20,000 × *g* at 4°C, 5 mg proteins were precleared for 1 h at 4°C with 20 μg GST proteins. The samples were incubated with 20 μg of immobilized GST fusion protein on beads overnight at 4°C. The beads were washed 5 times with lysis buffer and boiled in SDS loading buffer for 5 min at 95°C before WB.

Purified protein binding assay and binding affinity calculation. Free GST-Syt11 proteins were incubated with His-tagged EndoA1 in 500 μl HEKG buffer (in mM as follows: 20 HEPES, 1 EDTA, 50 KCl, pH 7.2) for 1 h at 4°C. Then 40 μl of 50% glutathione Sepharose beads was added and left on a rotating wheel for another 1 h at 4°C. The bound fraction on beads was collected for WB.

To calculate GST-Syt11 and EndoA1 binding affinity, increasing concentrations of GST-Syt11 (0-100 nM) were incubated with 20 nM His-tagged EndoA1. EndoA1 was pulled down with GST-Syt11, detected by anti-His tag antibody, and quantified using ImageJ. The bound fraction of EndoA1 was plotted and curve-fitted with GraphPad Prism 5.

For domain and peptide competition assays, GST-Syt11 protein was incubated with His-tagged EndoA1 along with C2 domains or peptides for 1 h at 4°C.

Peptide design, preparation, and application. The secondary structure of Syt11-C2B (291-428) was predicted by JPred (http://www.compbio.dundee.ac.uk/jpred/). Six peptides were designed according to their secondary structure (PP-1, RGELQVSLSYQPVAQRMTVVVLK; PP-2, ARHLPKMDITGLSGNPYVKVNV; PP-3, YYGRKRIAKKKTHVKKCTLNPIFN; PP-4, ESFIYDIPTDLLPDISIEFLVID; PP-5, FDRTTKNEVVGRLILGAHSVTTSG; and PP-6, AEHWREVCESPRKPVAKWHSLS). Their hydrophilic properties, molecular weights, and isoelectric points were analyzed, and they were synthesized by ChinaPeptide. Each peptide (1 mg) was first hydrated with 300 μl methanol, adjusted to 100 μM with ddH_20, aliquoted, and stored at –80°C. The hydrated peptides were used within 2 weeks.

To study the cell entry of peptides, FITC-conjugated PP-1 and PP-2 were synthesized. HEK293T cells were incubated for 3 h with 10 μM hydrated peptides, then for another 15 min with CellMask deep red dye (C10046, Invitrogen) to label the plasma membrane. Finally, the cells were fixed in 4% PFA for confocal observation. The cells were scanned under a Leica TCS SP8 confocal microscope with a 63× objective and 2.5× digital zoom. Series scanning with 0.4 μm slices on the *z* axis was used for 3D reconstitution.

For peptide application to cells, 10 μM hydrated peptide was added to the culture medium; and after 3 h, IP or FM4-64 uptake and discharge was assessed. For dialysis in the presynaptic structure of the calyx of Held, peptides were diluted to the desired concentration with presynaptic pipette solution. A double-blind strategy was adopted for capacitance recordings when examining the effects of PP-1 and PP-2.

Electrophysiological recordings from primary cultured hippocampal neurons. Electrophysiological recordings in cultured hippocampal neurons were performed after DIV14. For IPSC recording, 50 μM of D-APV and 20 μM of CNQX were added to the extracellular solution (in mM as follows: 140 NaCl, 5 KCl, 1.5 $CaCl_2$, 2 $MgCl_2$, 10 glucose, 10 HEPES-NaOH, pH 7.4, ~310 mOsm) to isolate inhibitory neurotransmissions. Glass pipettes were pulled at 2-4 MΩ and filled with intracellular solution (in mM as follows: 40 CsCl, 90 K-gluconate, 1.8 NaCl, 1.7 $MgCl_2$, 3.5 KCl, 0.05 EGTA, 2 MgATP, 0.4 Na_2-GTP, 10 phosphocreatine, 4

←

pHluorin and Syb2-pHluorin. Δcre-$\tau_{Syt1\text{-}pHluorin}$: 29.02 ± 1.32 s, 76 boutons from 3 experiments; cre-$\tau_{Syt1\text{-}pHluorin}$: 17.97 ± 0.71 s, 103 boutons from 3 experiments, $^{**}p = 0.0018$. Δcre-$\tau_{Syb2\text{-}pHluorin}$: 35.60 ± 1.90 s, 67 boutons from 3 experiments; cre-$\tau_{Syb2\text{-}pHluorin}$: 19.84 ± 0.87 s, 93 boutons from 3 experiments, $^{**}p = 0.0016$. Data are mean ± SEM. $^{***}p < 0.001$; Student's *t* test for ***B***, ***G***, ***J***, ***K***, ***N***, ***P***.

Table 1. *p* values for Figure 2

Time (s)	*p*	Mean 1	Mean 2	Difference	SE of difference	*t* ratio
p values of 10 Hz						
1	> 0.9999	1	1	4.91E-08	0.157286	3.12E-07
2	0.640606	0.731662	0.681431	0.050231	0.106339	0.472367
3	0.761669	0.623827	0.595563	0.028264	0.092218	0.306494
4	0.503278	0.575645	0.514566	0.061078	0.089983	0.678775
5	0.375126	0.496723	0.419473	0.07725	0.085605	0.902406
6	0.545574	0.491338	0.439213	0.052125	0.085112	0.612428
7	0.294225	0.482375	0.388753	0.093622	0.087455	1.07051
8	0.506605	0.427156	0.370797	0.056359	0.083688	0.673448
9	0.546551	0.423553	0.372397	0.051156	0.083735	0.610929
10	0.337478	0.397569	0.323591	0.073978	0.075704	0.977195
11	0.307297	0.416406	0.327565	0.088841	0.082986	1.07056
12	0.251039	0.406339	0.280077	0.126262	0.104209	1.21163
13	0.117312	0.41453	0.232101	0.182429	0.107349	1.6994
14	0.113204	0.390335	0.212136	0.178199	0.10354	1.72107
15	0.094801	0.385635	0.21061	0.175025	0.095756	1.82783
16	0.051183	0.383428	0.175129	0.208299	0.095219	2.18759
17	0.046242	0.4161	0.191363	0.224738	0.100077	2.24564
18	0.053249	0.390098	0.177235	0.212863	0.098325	2.16489
19	0.036187	0.379105	0.163751	0.215353	0.090299	2.38489
20	0.043582	0.373336	0.150398	0.222938	0.097805	2.27941
21	0.064605	0.352353	0.151121	0.201232	0.098003	2.05332
22	0.058929	0.360258	0.156727	0.203531	0.096619	2.10654
23	0.054497	0.357276	0.15431	0.202966	0.094334	2.15158
24	0.056944	0.338656	0.142199	0.196458	0.092394	2.1263
25	0.033314	0.352256	0.13638	0.215876	0.088779	2.43162
26	0.031132	0.365731	0.147722	0.218009	0.088269	2.46982
27	0.039441	0.354951	0.144623	0.210328	0.090033	2.33612
28	0.036042	0.339267	0.128377	0.21089	0.088343	2.38716
29	0.044715	0.336599	0.122111	0.214488	0.094705	2.26479
30	0.021769	0.345636	0.122996	0.22264	0.083366	2.67064
31	0.043347	0.337605	0.122441	0.215163	0.094267	2.28248
32	0.024639	0.34147	0.122007	0.219462	0.084368	2.60126
33	0.027981	0.346054	0.121248	0.224806	0.088861	2.52986
34	0.025479	0.347914	0.122837	0.225077	0.087157	2.58244
35	0.043129	0.324762	0.129131	0.195631	0.085602	2.28534
36	0.029869	0.355701	0.117777	0.237924	0.095432	2.49314
37	0.048044	0.319751	0.115741	0.20401	0.091739	2.22381
38	0.045959	0.325896	0.112762	0.213135	0.094763	2.24914
39	0.043317	0.327651	0.11233	0.215321	0.09432	2.28287
40	0.035811	0.319571	0.105549	0.214022	0.089519	2.3908
p values of 10 Hz						
1	> 0.9999	1	1	6.8545E-07	0.159797	4.29E-06
2	0.634952	0.671294	0.606118	0.0651763	0.135076	0.482516
3	0.773206	0.572223	0.535879	0.0363443	0.124328	0.292326
4	0.445884	0.544292	0.45354	0.0907522	0.116579	0.778461
5	0.364534	0.489954	0.387872	0.102082	0.109882	0.929016
6	0.027973	0.504593	0.298934	0.205659	0.0864307	2.37946
7	0.009586	0.458892	0.210802	0.24809	0.0861358	2.88022
8	0.004763	0.451743	0.176235	0.275507	0.0862202	3.19539
9	0.002844	0.426347	0.140253	0.286094	0.0835477	3.42432
10	0.005476	0.395599	0.136344	0.259255	0.0827478	3.13307
11	0.001703	0.395125	0.113387	0.281738	0.0771889	3.64999
12	0.002366	0.372854	0.098136	0.274718	0.0783693	3.50543
13	0.004681	0.351176	0.087612	0.263564	0.0822817	3.20319
14	0.004453	0.342723	0.090214	0.252509	0.0782868	3.22544
15	0.00495	0.339496	0.090093	0.249404	0.0784739	3.17818
16	0.008802	0.31796	0.088455	0.229505	0.0786231	2.91905
17	0.012703	0.316096	0.087211	0.228884	0.0831961	2.75114
18	0.005432	0.335934	0.085646	0.250288	0.0797941	3.13668
19	0.004008	0.349731	0.090001	0.25973	0.0793724	3.2723
20	0.004937	0.334691	0.090802	0.243889	0.0767091	3.1794

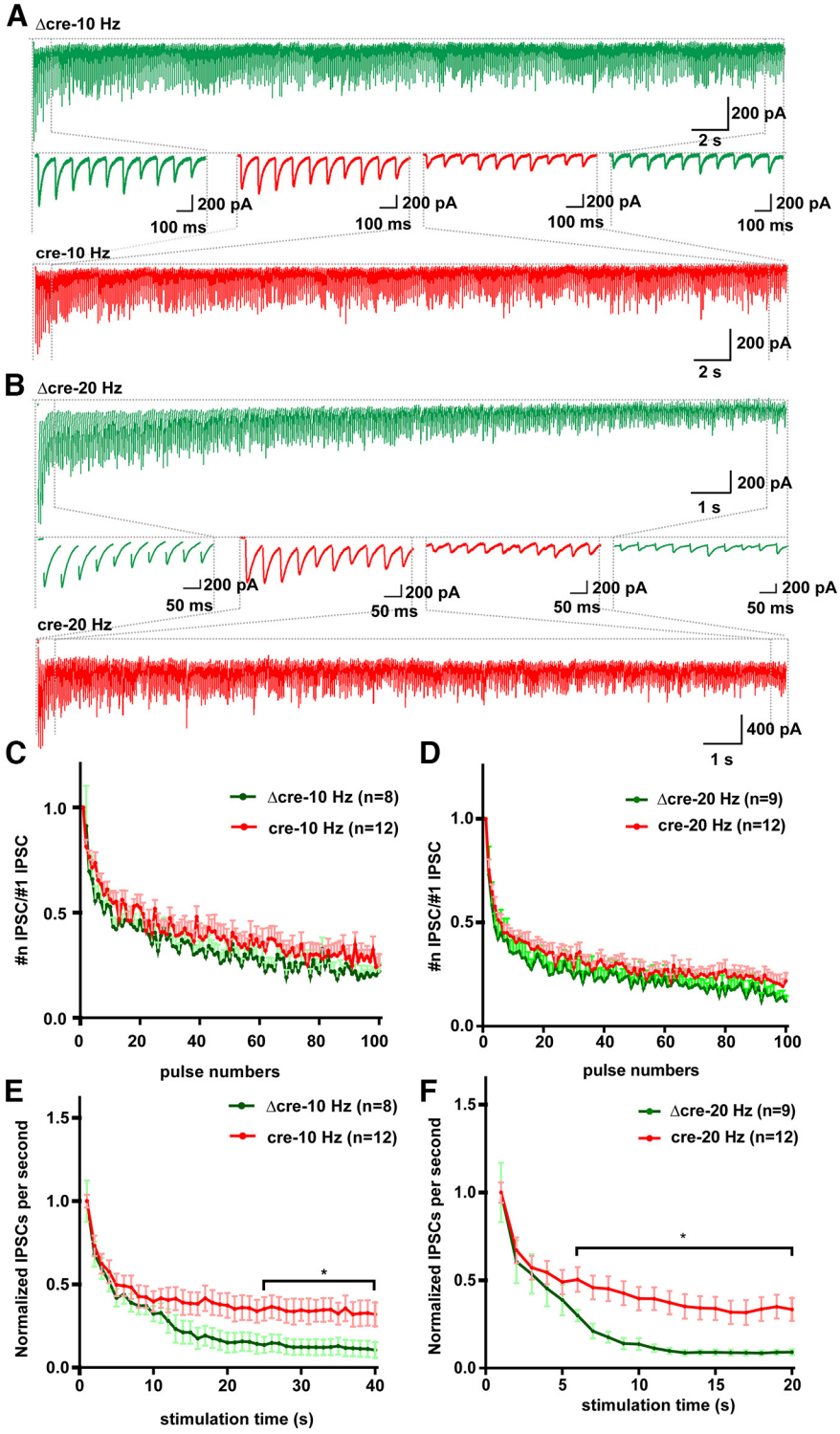

Figure 2. SV recycling accelerates during prolonged train stimulation at different frequencies in Syt11-KO neurons. ***A***, ***B***, Example traces of the eIPSCs in Δcre/cre treated neurons with 10/20 Hz stimulation. Total 400 stimulus traces included and the first/last 10 stimuli enlarged. ***C***, ***D***, The first 100 pulses of #n IPSC/#1 IPSC ratios at 10/20 Hz. ***E***, ***F***, 10/20 #n IPSC/#1 IPSC ratios within every s of 10/20 Hz stimulation were summed and normalized, and all the data in 40/20 s were plotted. Significant differences detected after 25/6 s for 10/20 Hz. *p* values are listed in Table 1. Data are mean ± SEM. $^*p < 0.05$; multiple *t* tests for ***E***, ***F***.

QX314-Cl, 10 HEPES-CsOH, pH 7.4, ~300 mOsm). Recordings were performed at room temperature (21°C-24°C). After breaking into the cells and establishing the whole-cell recording configuration, cells were kept at a holding potential of −70 mV throughout the recording. Access resistance was compensated to 3-5 MΩ during recording, and a concentric bipolar electrode was used to trigger the train stimulation (20 Hz). Data were acquired with an Axon 700B Multiclamp amplifier and analyzed by Igor 6.2 software 142 (WaveMetrics).

Slice preparation and electrophysiology at the calyx of Held. For capacitance recordings, transverse slices 200-μm-thick from 8- to 10-d-old C57/BL6 mice of either sex were cut on a vibratome (Leica VT 1200 s). Presynaptic capacitance was recorded at near-physiological

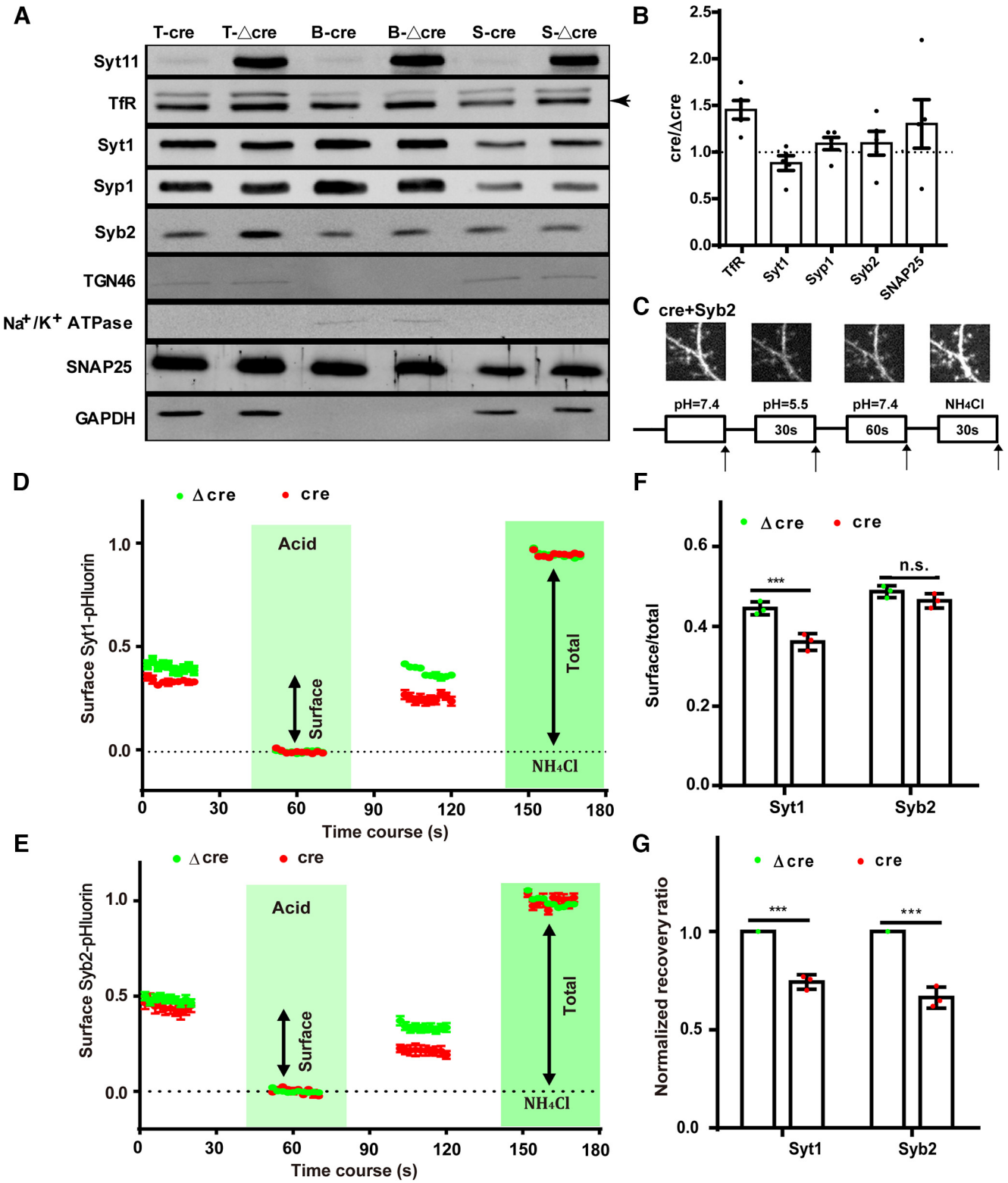

Figure 3. Membrane partition of TfR and Syt1 is altered in Syt11-KO neurons. ***A***, Plasma membrane fractionation using the Qproteome Plasma Membrane Protein Kit. T, Total lysate; B, resin-bound fraction; S, supernatant fraction. Syt1, Syp1, and Syb2 from the SV recycling pathway were investigated. Arrowhead indicates TfR. Na^+/K^+ ATPase and SNAP25 served as positive controls for plasma membrane proteins and presynaptic membrane. TGN 46 of the trans-Golgi network and cytosolic GAPDH served as negative controls. ***B***, Quantification of relative membrane fractions (cre/Δcre) as in ***A***. For each protein, the cell surface partition was calculated by the ratio of bound fraction to total fraction. Dashed line indicates the value 1, at which the membrane partition in Syt11-KO neurons is the same as the control. Increased TfR was retained on the plasma membrane in Syt11-KO neurons (1.44 ± 0.13, $^*p = 0.014$), while the partition of other proteins was not significantly changed (0.87 ± 0.08 in Syt1, $p = 0.26$). Data from five biological replicates ($n = 5$). ***C***, Protocol for assessing SV protein partition using pHluorin-tag (Syb2 as an example). The first 10 frames were acquired in standard imaging buffer to obtain the baseline; then the pHluorin signals were quenched by acid treatment (pH 5.5 for 30 s). The cells were then bathed in standard imaging buffer (60 s) for recovery of the surface signal, and the total level of pHluorin protein in the bouton was assessed by NH_4Cl perfusion for 30 s. Arrows indicate the starting points for acquisition of 10 frames at 2 s intervals. Scale bar, 5 μm. ***D***, ***E***, Averaged traces showing Syt1-pHluorin and Syb2-pHluorin signals during treatments. ***F***, Quantification of surface Syt1-pHluorin and Syb2-pHluorin. The surface ratio of Syt1-pHluorin was 0.4449 ± 0.014 in control (Δcre, 77 boutons from 3 experiments) and 0.3609 ± 0.014 in Syt11-KO boutons

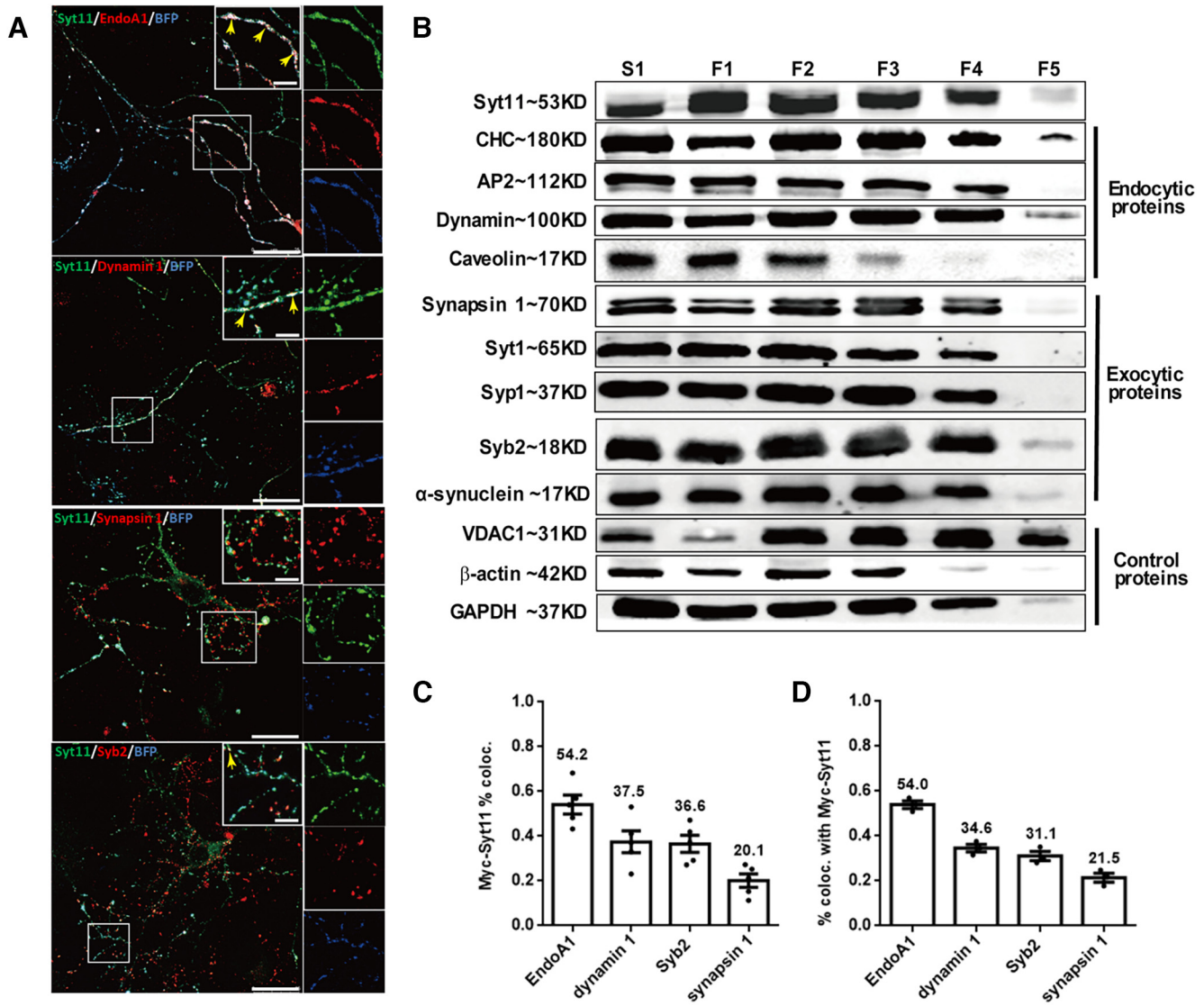

Figure 4. Syt11 is localized to the SV recycling pathway. ***A***, Myc-Syt11 partially colocalized with synapsin 1, Syb2, EndoA1, and dynamin 1 at presynaptic hippocampal terminals. Top right inset (in each panel), An enlargement. Scale bar, 5 μm. Arrows indicate colocalized puncta. Scale bars: original images, 25 μm. ***B***, Synaptosome fractionation of rat cortex by Percoll gradient centrifugation. S1, Soluble fraction; F1-F5, myelin, membranes, synaptosomes and membranes, synaptosomes, and mitochondria. Endocytic and synaptic proteins in presynaptic terminals were investigated. Voltage-dependent anion-selective channel protein 1 (VDAC1) served as a marker of mitochondria. ***C***, ***D***, Analysis of colocalization of myc-Syt11 with EndoA1, Syb2, synapsin 1, dynamin 1 in neuronal dendrites by Pearson's coefficient. Left, The percentage of myc-Syt11 colocalized with various proteins. Right, The percentage of these proteins with myc-Syt11. All data are from at least five frames of images from three independent experiments.

temperature (33°C-35°C) or room temperature (22°C-24°C) with ACSF containing the following (in mM): 105 NaCl, 2.5 KCl, 25 $NaHCO_3$, 3 myo-inostol, 2 Na-pyruvate, 1.25 NaH_2PO_4, 0.4 ascorbic acid, 25 D-glucose, 1 $MgCl_2$, 2 $CaCl_2$, 0.001 TTX, and 20 tetraethylammonium at pH 7.4 when gassed with 95% O_2 and 5% CO_2. The osmolarity of this solution was in the range of 295-320 Osm. The presynaptic pipette (3-5 MΩ) solution contained the following (in mM): 125 Cs-gluconate, 20 CsCl, 4 MgATP, 10 Na_2-phosphocreatine, 0.3 GTP, 10 HEPES, and 0.05 BAPTA (pH 7.2 adjusted with CsOH). Presynaptic whole-cell recordings were made with an EPC-10 amplifier (HEKA), with series resistance <15 MΩ compensated by 60%. The holding potential of −80 mV was corrected for a liquid junction potential of −11 mV between the extracellular and pipette solutions. A sinusoidal stimulus was applied in addition to the DC holding potential. The peak-to-peak voltage of the sine wave was <60 mV to avoid activating Ca^{2+} currents. The resulting current was processed using the Lindau–Neher technique to give estimates of the membrane capacitance, membrane conductance, and series conductance. The sine wave frequency was 1000 Hz. Data are expressed as mean ± SEM, and one-way ANOVA was used. All data were analyzed with Igor Pro-6.2 (WaveMetrics).

Experimental design and statistical analysis. All experiments were replicated biologically for at least 3 times. Data are presented as mean ± SEM, and statistical analysis was performed using GraphPad Prism software. Statistical comparisons were made using the two-tailed unpaired *t* test, one-way ANOVA with Dunnett's analysis, or two-way ANOVA with Sidak analysis. Sidak's *post hoc* test was used. Numbers of experiments or analyzed samples are provided in the corresponding figure legends. *p* values < 0.05 were considered significant.

←

(cre, 65 boutons from 3 experiments). ***$p = 0.0008$. For Syb2-pHluorin, the ratios were 0.4868 ± 0.0840 in Δcre and 0.4637 ± 0.0231 in cre, $p = 0.2757$. The surface distribution of Syt1 decreased 18.88% after Syt11 depletion, while Syb2 did not change. ***G***, Relative surface fluorescence recovery ratios of Syb2-pHluorin (0.7424 ± 0.0649) and Syt1-pHluorin (0.6631 ± 0.0375) in the absence of Syt11. Data are mean ± SEM. *$p < 0.05$; ***$p <$ 0.001; column statistics was used to compare with value 1.0 in ***B***; Student's *t* test for ***F***, ***G***.

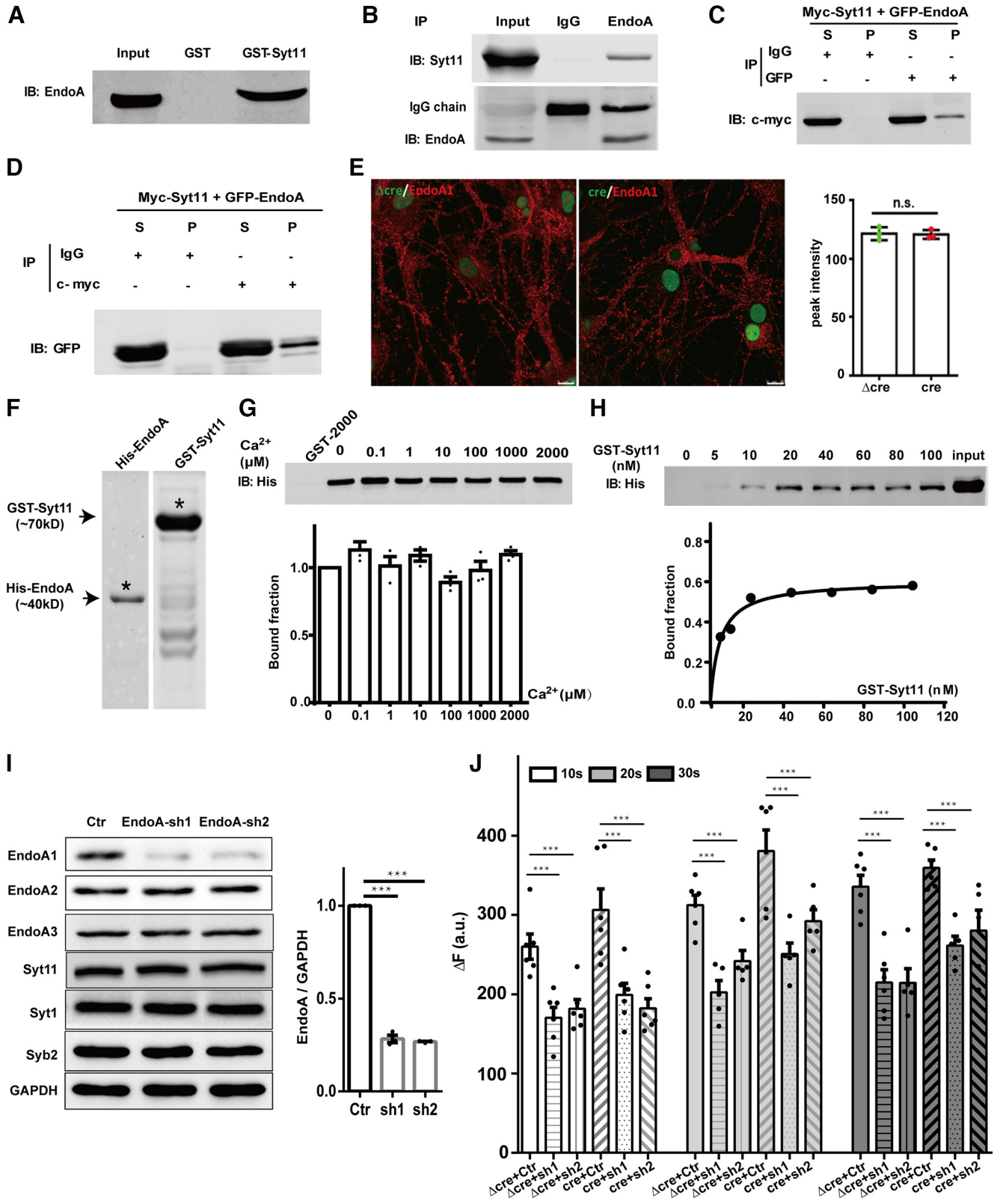

Figure 5. Syt11 directly interacts with EndoA1 with high affinity in a Ca^{2+}-independent manner. ***A***, ***B***, GST pull-down with GST-Syt11 and IP with EndoA1 antibody in mouse brain lysates. Input fraction (1% of total) and bound fraction were immunoblotted with EndoA1 or Syt11 antibody. ***C***, ***D***, Coimmunoprecipitation of myc-Syt11 and GFP-EndoA1 in HEK293T cells. ***E***, Cre or Δcre neurons (green) were stained with EndoA1 antibody (red). The same parameters were used for image capture and the peak intensities of ROIs quantified. Scale bars, 10 μm. ***F***, Purification of His-tagged EndoA1 and GST-Syt11 revealed by Coomassie staining. ***G***, Syt11-EndoA1 binding is Ca^{2+}-independent. ***H***, Affinity of the Syt11-EndoA1 interaction. A constant concentration of free EndoA1 (20 nM) was incubated with different concentrations of free GST-Syt11 (0-100 nM) to determine the K_d value. Curve-fitting by saturation binding equations ($Y = 0.6*X/(4.8 + X)$) revealed one specific binding site with a K_d of 4.79 nM. ***I***, The KD efficiency of EndoA1 in neurons treated with lentivirus (one-way ANOVA: $F = 1252$, $^{***}p < 0.0001$; sh-1, 28.3% of nontargeting control (Ctr), $^{***}p < 0.0001$; sh-2, 26.7% of Ctr, $^{***}p < 0.0001$). EndoA2/A3 and other synaptic protein (Syt11, Syt1, Syb2) expression did not change after EndoA1 KD. ***J***, EndoA1-KD reversed the FM4-64-uptake phenotype in Syt11-KO neurons. 10 s (one-way ANOVA: $F = 13.57$, $^{***}p < 0.001$): Δcre + sh1 versus Δcre + Ctr, 34. 48% decreased,

Results

Syt11-KO accelerates endocytosis in neuronal terminals without affecting exocytosis

Previously, we showed that Syt11-KD accelerates neuronal endocytosis in both the somata of DRG neurons and the terminals of hippocampal neurons (Wang et al., 2016). In this study, we analyzed the function of Syt11 by investigating Syt11-KO synapses. Primary hippocampal neurons from a floxed Syt11 knock-in mouse strain (Shimojo et al., 2019) were infected with lentivirus-expressing cre recombinase to generate Syt11-KO cells. A truncated, catalytically inactive Δcre served as a negative control. The KO efficiency reached 94.3% (Fig. 1*A*,*B*) without affecting the expression of other endocytic proteins (dynamin 1 and EndoA1), Syt isoforms (Syt1 and Syt4), or a SV protein [synaptobrevin 2 (Syb2)].

To investigate the endocytic phenotype in Syt11-KO neurons, we first used FM4-64 dye to assess vesicle endocytosis and exocytosis at neuronal terminals. The dye was applied extracellularly during 60 s of stimulation with 100 mM K^+ at 37°C followed by three 60 s washes and then unloaded by a train of 800 APs at 40 Hz (Fig. 1*C*). The FM4-64 discharged from Syt11-KO terminals increased by 104.67% (Fig. 1*D*,*E*,*G*). When the FM4-64 discharge signal was normalized to the total dischargeable amount, no difference in exocytic kinetics was found between Syt11-KO and control cells (Fig. 1*F*). To make sure that Syt11-KO did not affect exocytosis, we used an overstimulation protocol (Verstreken et al., 2008; Iwabuchi et al., 2014) and included FM4-64 during and 3 min after stimulation to stain most of the recycling vesicles, followed by a train of stimuli to evoke exocytosis (800 APs at 40 Hz; Fig. 1*H*). The FM4-64 discharge showed that exocytosis in Syt11-depleted neurons was not altered (Fig. 1*I*,*J*), consistent with previous reports that Syt11 is not involved in regulating evoked exocytosis (Wang et al., 2016; Shimojo et al., 2019). As the train stimulation depleted the recycling pool, this result also showed that the size of the recycling pool in Syt11-KO neurons was unaffected. Comparatively, a remarkable increase in FM4-64 uptake occurred in Syt11-KO boutons at various durations of electrical stimulation (40 Hz for 10, 20, or 30 s) with negligible spontaneous uptake and nonspecific FM4-64 staining (30 s, Fig. 1*K*). Furthermore, we examined endocytosis kinetics by introducing pHluorin-tagged Syt1 (Syt1-pHluorin) or Syb2 (Syb2-pHluorin) into hippocampal neurons. pHluorin is a pH-sensitive variant of GFP, which fluoresces in the neutral environment after exocytosis (Betz and Bewick, 1992; Miesenbock et al., 1998; Zhu et al., 2009). After a train of 10 Hz 500 AP stimulation, both Syt1-pHluorin and Syb2-pHluorin endocytosed faster after Syt11 depletion (Fig. 1*L*–*P*). Together, these results revealed an inhibitory role of Syt11 in SV endocytosis without directly affecting exocytosis.

Syt11-KO enhances neurotransmission during prolonged stimulations

As endocytosis is an important stage of vesicle recycling which largely determines vesicle availability during sustained neuronal activity (Li et al., 2005; Qiu et al., 2015), we recorded the eIPSC corresponding to 400 stimuli at different frequencies (10/20 Hz) in primary hippocampal neurons (Fig. 2; Table 1). It seemed that loss of Syt11 had no impact on the first 100 AP-evoked releases at 10 and 20 Hz (Fig. 2*C*,*D*). However, our results showed that Syt11-KO significantly enhanced the IPSCs when stimulation duration was extended longer than 25 and 6 s corresponding to 10 and 20 Hz stimulation (Fig. 2*E*,*F*). Together, our observations provided strong supporting evidence that Syt11 loss caused acceleration of endocytosis increases the reused vesicle availability.

Membrane partition of synaptic proteins is defective in Syt11-KO neurons

We have proposed that Syt11 inhibits neuronal endocytosis to ensure the precise recycling of synaptic proteins and membranes (Wang et al., 2016). In the somata of DRG neurons, downregulation of Syt11 leads to excessive membrane retrieval after evoked exocytosis. Here, we set out to investigate the retrieval of synaptic proteins by examining their membrane partition in hippocampal neurons. First, we used a biochemical surface protein extraction method to distinguish the plasma membrane fraction from the intracellular fraction. Syt11 was present in the plasma membrane fraction (Fig. 3*A*). We found that more TfR was retained on the plasma membrane in Syt11-KO neurons (Fig. 3*A*,*B*, $^*p = 0.014$, *t* test), consistent with the increased transferrin uptake previously reported (Wang et al., 2016). Synaptophysin 1 (Syp1), Syb2, and SNAP25 were not affected, while Syt1 on the plasma membrane tended to decrease after Syt11-KO ($p = 0.26$, *t* test). Na^+/K^+ ATPase (a plasma membrane marker) served as a positive control for the membrane fraction (Fig. 3*A*), while the intracellular membrane protein TGN 46 (a Golgi apparatus marker) and the cytosolic protein GAPDH served as positive controls for the intracellular fraction.

Notably, the above experiments used the plasma membrane fraction of the entire neuron, including the somata and neurites. To examine the synaptic protein partition in nerve terminals, we used Syb2-pHluorin and Syt1-pHluorin to investigate their surface partition in Syt11-KO terminals. The surface fraction of each protein was estimated by a round of acid, neutral, and alkaline treatments (Fig. 3*C*). We found that the surface partition ratio of Syt1, but not Syb2, significantly decreased after Syt11 depletion (by 18.88%, Fig. 3*D*–*F*). Furthermore, the surface fluorescence recovery of both Syb2-pHluorin (0.7424 ± 0.0649) and Syt1-pHluorin (0.6631 ± 0.03747) were impaired in Syt11-KO neurons when cells were switched from acidic solution back to standard buffer (Fig. 3*G*).

Syt11 is localized to synapses

High levels of Syt11 mRNA and protein expression have been reported in many regions of the rodent brain (von Poser et al., 1997; Mittelsteadt et al., 2009; Shimojo et al., 2019). Here, we

←

$^{***}p < 0.001$; Δcre + sh2 versus Δcre + Ctr, 30.18% decreased, $^{***}p < 0.001$; cre + sh1 versus cre + Ctr, 34.97% decreased, $^{***}p < 0.001$; cre + sh2 versus cre + Ctr, 40.50% decreased, $^{***}p < 0.001$. 289 boutons from 6 experiments in Δcre + Ctr, 272 boutons from 6 experiments in Δcre + sh1, 268 boutons from 6 experiments in Δcre + sh2; 282 boutons from 6 experiments in cre + Ctr, 309 boutons from 6 experiments in cre + sh1, 291 boutons from 6 experiments in Δcre + sh2. 20 s (one-way ANOVA: $F = 14.3$, $^{***}p < 0.001$): Δcre + sh1 versus Δcre + Ctr, 35.23% decreased, $^{***}p < 0.001$; Δcre + sh2 versus Δcre + Ctr, 22.56% decreased, $^{***}p < 0.001$; cre + sh1 versus cre + Ctr, 34.16% decreased, $^{***}p < 0.001$; cre + sh2 versus cre + Ctr, 23.22% decreased, $^{***}p < 0.001$; 313 boutons from 6 experiments in Δcre + Ctr, 295 boutons from 5 experiments in Δcre + sh1, 329 boutons from 5 experiments in Δcre + sh2; 331 boutons from 6 experiments in cre + Ctr, 307 boutons from 5 experiments in cre + sh1, 335 boutons from 5 experiments in Δcre + sh2. 30 s (one-way ANOVA: $F = 22.33$, $^{***}p < 0.001$): Δcre + sh1 versus Δcre + Ctr, 34.00% decreased, $^{***}p < 0.001$; Δcre + sh2 versus Δcre + Ctr, 36.14% decreased, $^{***}p < 0.001$; cre + sh1 versus cre + Ctr, 27.26% decreased, $^{***}p < 0.001$; cre + sh2 versus cre + Ctr, 22.03% decreased, $^{***}p < 0.001$. 323 boutons from 6 experiments in Δcre + Ctr, 259 boutons from 6 experiments in Δcre + sh1, 379 boutons from 5 experiments in Δcre + sh2; 268 boutons from 6 experiments in cre + Ctr, 301 boutons from 5 experiments in cre + sh1, 276 boutons from 5 experiments in Δcre + sh2. Data are mean ± SEM. $^{***}p < 0.001$; Student's *t* test for ***E***.

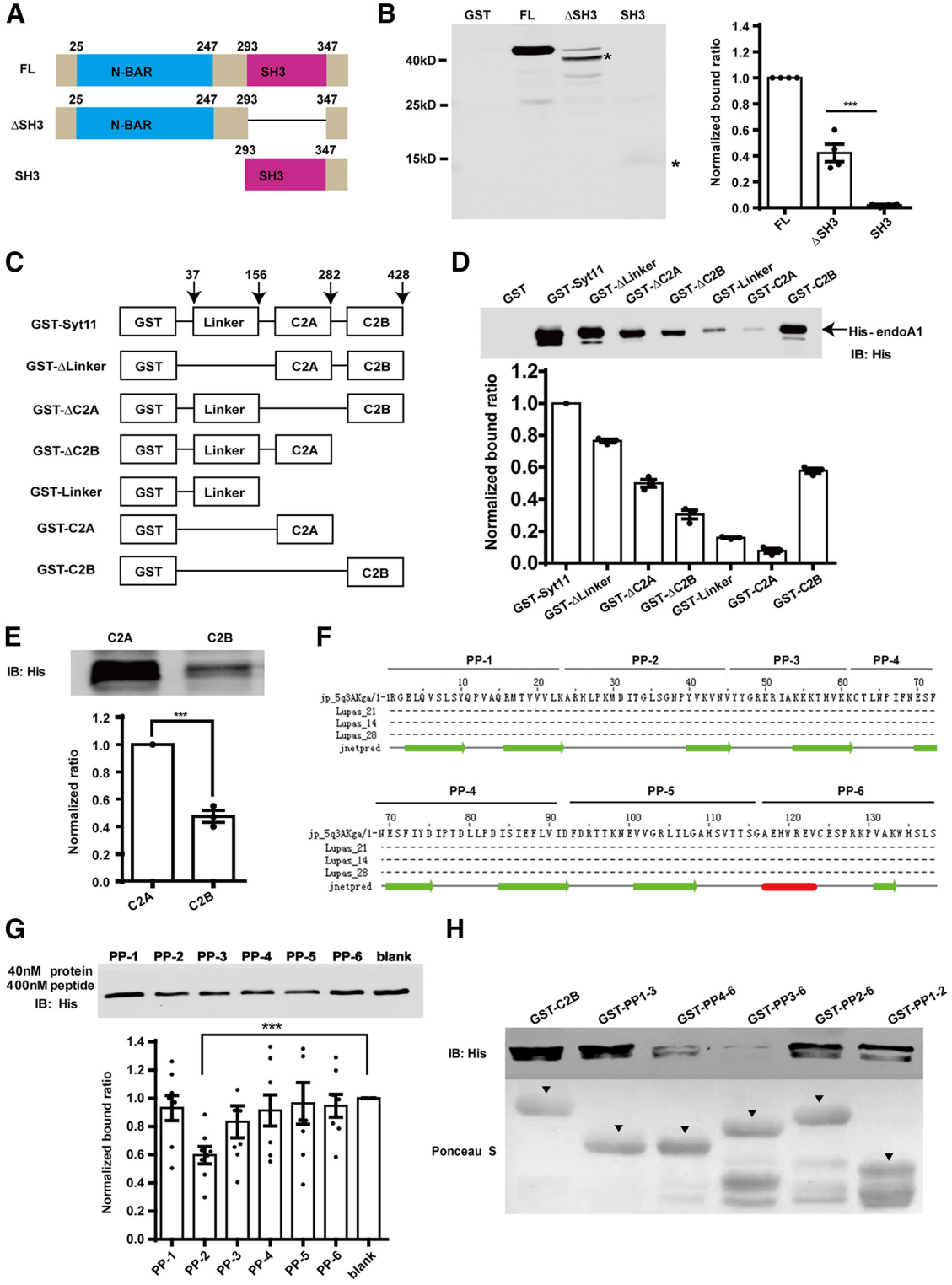

Figure 6. Domain requirement of Syt11-EndoA1 binding. ***A***, ***B***, Construction of His-tagged EndoA1 mutation (amino acid numbers of N-BAR and SH3 domains are indicated). The SH3 domain is not necessary for Syt11–EndoA1 binding. ***C***, Diagram of Syt11 cytosolic domains with GST tag. ***D***, C2B domain is sufficient for Syt11–EndoA1 interaction (one-way ANOVA: $F = 549$, $^{***}p < 0.001$). ***E***, Competition of the same concentration of C2B domain with Syt11 binding to EndoA1. The C2B domain inhibited 52.6% of the interaction compared with C2A. ***F***, Secondary structure prediction of Syt11-C2B by JPred. C2B is composed of eight β-sheets (green arrows) and one α-helix (red bar). Peptides 1-6 were designed according to the secondary structure prediction. ***G***, Peptide 2 (PP-2) was used to block the Syt11–EndoA1 interaction, and PP-2 reduced the Syt11–EndoA1 binding by 38.5% *in vitro* (one-way ANOVA: $F = 3.2$, $^{*}p = 0.013$). ***H***, Different GST-tagged C2B domain truncations were used for GST pull-down. The PP-2 sequence was indispensable for this binding. Ponceau S staining shows equal volumes of GST-tagged proteins (triangles). Data are from at least three independent experiments and presented as mean ± SEM. $^{***}p < 0.001$; Student's *t* test for ***E***; one-way ANOVA for ***B***, ***D***, ***G***,

Table 2. Peptide information

	Amino acid sequence	Hydrophilicity	MW	Isoelectric point
PP-1	rgelqvslsyqpvaqrmtvvvlk	−0.1	2602.1	10.5
PP-2	arhlpkmditglsgnpyvkvnv	0.0	2409.84	10.2
PP-3	yygrkriakkkthvkkctlnpifn	0.3	2907.53	11.1
PP-4	ctlnpifnesfiydiptdllpd	−0.3	2540.87	2.8
PP-5	isieflvidfdrttknevvgrlilgahsvttsg	−0.1	3589.11	5.5
PP-6	aehwrevcesprkpvakwhsls	0.3	2632.99	9.0

determined the subcellular localization of Syt11 in hippocampal terminals. Synapsin 1 and Syb2 were SV proteins, while EndoA1 and dynamin 1 labeled the endocytic pathway. Syt11 was localized at terminals, and partly colocalized with synapsin 1, Syb2, EndoA1, and dynamin 1 (Fig. 4*A*,*C*,*D*). Among these, Syt11 colocalized most extensively with EndoA1. These results suggested that Syt11 is a presynaptic protein involved in SV recycling.

We also investigated the Syt11 distribution biochemically. Percoll gradient centrifugation was applied to isolate different membrane fractions, including intact synaptosomes, from rat brain (Dunkley et al., 2008). Synapsin 1, Syt1, Syp1, Syb2, and α-synuclein were monitored to label presynaptic structures. Clathrin heavy chain, adaptor protein 2 (AP2), dynamin 1, and caveolin marked endocytic pathways. Voltage-dependent anion-selective channel protein 1 served as a marker of mitochondria, while β-actin and GAPDH were cytosolic. The high levels of endocytic proteins in the synaptosome fraction indicated active CME, but not caveolin-mediated endocytosis in synapses. Syt11 was enriched in several membrane fractions but not in mitochondria (Fig. 4*B*). The abundance of Syt11 protein in synaptosomes suggested important physiological functions of Syt11 in synapses. All these results showed that Syt11 is distributed in presynaptic structures, and is associated with SV recycling.

Syt11 interacts directly with EndoA1 through the C2B domain

To understand the molecular mechanism of Syt11 regulation during SV endocytosis, we sought for the proteins that interact with Syt11. GST pull-down experiments with mouse brain homogenates identified EndoA1, a crucial endocytic protein that recruits synaptojanin and dynamin 1 at a late stage of SV endocytosis (Milosevic et al., 2011; Sundborger et al., 2011), as a binding partner of GST-Syt11 (Fig. 5*A*). To investigate whether their interaction occurs *in vivo*, coimmunoprecipitation assays were performed using EndoA1 antibody (Fig. 5*B*). Syt11 was found in the same immune complex as EndoA1. We further confirmed their binding in HEK293T cells by coexpressing myc-Syt11 and EndoA1-GFP. Syt11 and EndoA1 immunoprecipitated with each other using either myc or GFP antibody (Fig. 5*C*,*D*). However, EndoA1 expression in nerve terminals was not affected in Syt11-KO neurons (Fig. 5*E*).

To determine whether the binding of Syt11 to EndoA1 was direct, we purified GST-Syt11 and His-EndoA1 *in vitro* (Fig. 5*F*), and found that Syt11 interacted with EndoA1 directly in a Ca^{2+}-independent manner (from 0 to 2 mM, Fig. 5*G*). The affinity of their interaction was measured by keeping the concentration of EndoA1 constant (20 nM) while varying that of Syt11. Curve-fitting analysis revealed one binding site with high affinity (K_d = 4.79 nM, Fig. 5*H*). Together, our data revealed a strong interaction between Syt11 and EndoA1.

To investigate whether Syt11 inhibits SV endocytosis through EndoA1, we specifically knocked down EndoA1 in neurons using two shRNAs (Fig. 5*I*; sh-1, 28.3% of nontargeting control (Ctr); sh-2, 26.7% of Ctr), without affecting EndoA2/3 and other synaptic proteins Syt11, Syt1, and Syb2. EndoA1-KD reduced the FM4-64 uptake in the control groups (Fig. 5*J*), consistent with its reported effect on SV endocytosis (Zhang et al., 2015a). EndoA1-KD significantly reversed the increased FM4-64 uptake with various durations of electrical stimulation (40 Hz for 10, 20, or 30 s) in the Syt11-KO cells (Fig. 5*J*). The partial reversal was likely because of the incomplete KD of EndoA1 (by ~70%, Fig. 5*I*). These data suggested that EndoA1 is a key target of Syt11 during SV endocytosis.

Next, we mapped the binding domains of Syt11 and EndoA1. EndoA1 is one of the SH3 domain-containing proteins. Structurally, EndoA1 possesses an N-terminal BAR domain and a C-terminal SH3 domain. Its SH3 domain binds the proline-rich motif (PXXP) in multiple synaptic proteins, including synaptojanin (de Heuvel et al., 1997; Micheva et al., 1997a), amphiphysin (Micheva et al., 1997b), dynamin (Ringstad et al., 1997; Anggono and Robinson, 2007), voltage-gated Ca^{2+} channels (Pechstein et al., 2015), vesicular glutamate transporter type 1 (Vinatier et al., 2006), and intersectin (Chen et al., 2003). We tested whether Syt11 also binds the SH3 domain since four PXXP sites were found in Syt11. We constructed two deletion mutants of EndoA1, ΔSH3 and SH3 (Fig. 6*A*), and found that ΔSH3, but not SH3, bound Syt11, albeit with a lower affinity than full-length Syt11 (Fig. 6*B*). This result showed that Syt11 interacts with the N-terminal sequence of EndoA1.

Since EndoA1 is a peripheral membrane protein without a transmembrane domain, we reasoned that their interaction takes place on the cytosolic part of Syt11, we constructed a series of Syt11 cytosolic domains: GST-Syt11 [amino acids (a.a.) 37-428, covering the entire cytosolic region], GST-Δlinker (a.a. 157-428), GST-ΔC2A (a.a. 37-156 and 283-428), GST-ΔC2B (a.a. 37-282), GST-Linker (a.a. 37-156), GST-C2A (a.a. 157-282), and GST-C2B (a.a. 283-429) (von Poser et al., 1997). We found that the C2B domain mainly bound EndoA1 while the linker region and the C2A domain showed weak interaction (Fig. 6*C*,*D*).

To verify that C2B is the binding domain in Syt11, we used the C2A or C2B domain (cleaved from GST-C2A or GST-C2B by thrombin) to compete with the GST-Syt11–EndoA1 binding using equal concentrations of C2A or C2B (100 nM) and GST-Syt11 (100 nM). The C2B domain inhibited 52.6% of the Syt11–EndoA1 binding when normalized to C2A (Fig. 6*E*).

EndoA1-binding peptide derived from the C2B domain mimics Syt11 inhibition in SV endocytosis

Since several proteins, such as AP2 (Zhang et al., 1994) and SV2 (Schivell et al., 1996), are known to bind the C2B domain of the Syt family, we set out to narrow down the EndoA1 binding sequence in the C2B domain of Syt11. Six peptides covering the 137 amino acids of the C2B domain were designed according to the JPred prediction of secondary structures (Fig. 6*F*). Among these, the second peptide (PP-2, a.a. 314-336, ARHLPKMDITGLSGNPYVKVNV) significantly inhibited the Syt11-EndoA1 interaction (by 38.5%, Fig. 6*G*). We also constructed C2B truncations based on these peptides (Fig. 6*H*). Consistently, truncations that included the PP-2 sequence (GST-C2B, GST-PP1-3, GST-PP2-6, and GST-PP1-2) all bound EndoA1 while truncations lacking the PP-2 sequence (GST-PP4-6 and GST-PP3-6) failed to bind EndoA1. These results demonstrated that the C2B domain binds EndoA1 through the PP-2 sequence.

To understand the functional role of the Syt11–EndoA1 interaction in the cell, we first investigated whether PP-2 competes with this binding *in vivo*. Since PP-2 is positively charged

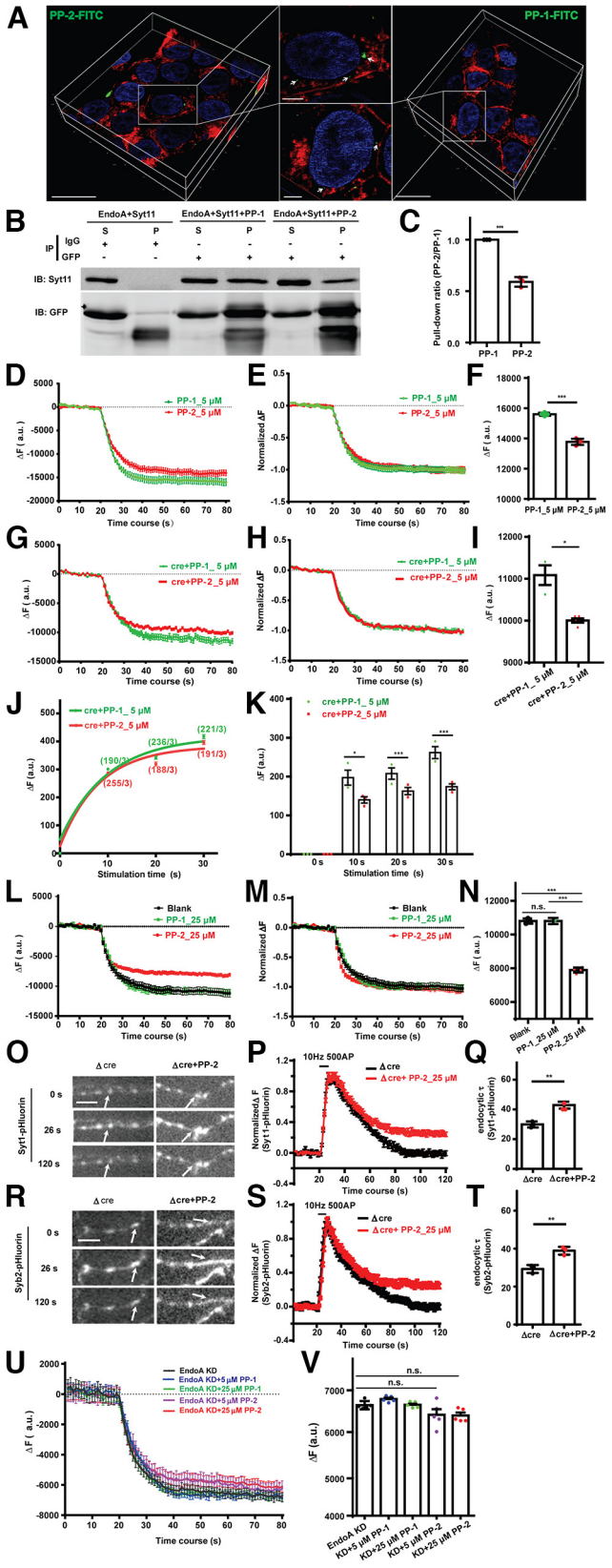

Figure 7. Extracellular application of PP-2 inhibits SV endocytosis via EndoA1 in hippocampal neuron terminals. ***A***, FITC-conjugated peptides entered cells and CellMask deep red marked plasma membrane. All the sections were reconstructed to form a 3D image. Blue represents DAPI for nucleus. Arrows, FITC-conjugated peptide puncta inside cells. Scale bars: left and right panels, 20 μm; middle subpanels, 5 μm. ***B***, ***C***, Treatment with 5 μM PP-1 (control) or PP-2 for 3 h blocked coimmunoprecipitation of Syt11 and EndoA1 in HEK293T cells. PP-2 decreased the interaction by 41.1% compared with PP-1. ***D–F***, FM4-64 uptake and discharge in WT hippocampal neurons treated with 5 μM PP-1 or PP-2 for 3 h. Quantification analysis shows that PP-2 inhibited terminal endocytosis by 11.7% compared with the PP-1 control (15,605 ± 50.36 with PP-1, 85 boutons from 4 experiments; 13,779 ± 100.60 with PP-2, 91 boutons from 4 experiments, $^{***}p < 0.001$), without affecting exocytosis. ***G–I***, Syt11-KO neurons were incubated with 5 μM PP-1 or PP-2 for 3 h before FM4-64 uptake and discharge experiments. Quantification shows that PP-2 decreased terminal endocytosis by 9.75% compared with the PP-1 control (11,085 ± 235.1 with PP-1, 70 boutons from 3 experiments; 10,004 ± 49.74 with PP-2, 216 boutons from 5 experiments, $^{**}p = 0.0011$), without affecting exocytosis. ***J***, ***K***, FM4-64 uptake in Syt11-KO neurons after electrical stimulation (40 Hz) for 10, 20, or 30 s. PP-2 significantly reduced FM4-64 uptake compared with PP-1 (10 s PP-1, 197.8 ± 19.5, 190 boutons from 3 experiments; 10 s PP-2, 140.0 ± 8.5, 255 boutons from 3 experiments, $^{*}p = 0.011$; 20 s PP-1, 207.1 ± 14.7, 236 boutons from 3 experiments; 20 s PP-2, 162.7 ± 9.6, 188 boutons from 3 experiments, $^{***}p < 0.001$; 30 s PP-1, 261.3 ± 15.2, 221 boutons from 3 experiments; 30 s PP-2, 174.5 ± 7.7, 191 boutons from 3 experiments, $^{***}p < 0.001$). ***L–N***, WT hippocampal neurons were treated with 25 μM PP-1 or PP-2 before FM4-64 uptake and discharge experiments. Quantification analysis shows that 25 μM PP-2 significantly inhibited terminal endocytosis to 73.08% of the blank control ($^{***}p < 0.001$) or 74.07% of PP-1 treatment ($^{***}p < 0.001$) (10,803 ± 42.87 with blank, 43 boutons from 3 experiments; 10,805 ± 21.90 with PP-1, 52 boutons from 3 experiments; 7895 ± 25.11 with PP-2, 98 boutons from 5 experiments), without affecting exocytosis. ***O–T***, The endocytic τ of Syt1-pHluorin and Syb2-pHluorin in control group (Δcre) or 25 μM PP-2-treated neurons (Δcre-$\tau_{Syt1\text{-}pHluorin}$: 29.94 ± 1.16 s, 67 boutons from 3 experiments; Δcre + PP-2-$\tau_{Syt1\text{-}pHluorin}$: 42.89 ± 1.33 s, 72 boutons from 3 experiments; $^{**}p = 0.0018$; Δcre-$\tau_{Syb2\text{-}pHluorin}$: 29.27 ± 1.31 s, 89 boutons from 3 experiments; Δcre + PP-2-$\tau_{Syb2\text{-}pHluorin}$: 38.89 ± 1.20 s, 101 boutons from 3 experiments, $^{**}p = 0.0048$). ***U***, ***V***, EndoA1-KD neurons treated with 5 or 25 μM of PP-1 or PP-2. The releasable amounts of FM4-64 were calculated, and no significant difference was found between each group (one-way ANOVA: $F = 1.86$, $p = 0.16$; EndoA1-KD = 6647 ± 18.39, 73 boutons from 5 experiments; EndoA1-KD + 5 μM PP-1: 6791 ± 19.57, 83 boutons from 5 experiments; EndoA1-KD + 25 μM PP-1: 6656 ± 25.22, 79 boutons from 5 experiments; EndoA1-KD + 5 μM PP-2: 6414 ± 32.50, 75 boutons from 5 experiments; EndoA1-KD + 25 μM PP-2: 6399 ± 47.19, 80 boutons from 5 experiments). Data are mean ± SEM. $^{*}p < 0.05$; $^{**}p < 0.01$; $^{***}p < 0.001$; Student's *t* test for ***C***, ***F***, ***I***, ***K***, ***Q***, ***T***; one way ANOVA for ***N***, ***V***.

(isoelectric point, 10.2, Table 2), we tested whether it enters cells via an electrostatic interaction with the plasma membrane. PP-1 served as a negative control as it shared hydrophilic properties, molecular weight, and isoelectric point (10.6, Table 2) with PP-2. Both peptides were tagged with FITC, and CellMask deep red dye was used to mark the cell membrane. Indeed, PP-1 and PP-2 were able to enter HEK293T cells (Fig. 7*A*). Next, we tested the effect of PP-2 in HEK293T cells expressing myc-Syt11 and EndoA1-GFP. Coimmunoprecipitation experiments showed that application of PP-2 efficiently blocked the Syt11–EndoA1 interaction by 41.1% when normalized to PP-1 (Fig. 7*B*,*C*). This result showed that PP-2 inhibits Syt11–EndoA1 binding in the cell.

Next, we explored the physiological function of the Syt11–EndoA1 interaction. There are two possibilities. One is that Syt11 is recruited to endocytic sites by EndoA1 and inhibits other proteins involved in SV endocytosis. In this case, application of PP-2 would mimic the Syt11-KO phenotype and accelerate SV endocytosis. The other possibility is that Syt11 inhibits EndoA1, leading to inhibition of SV endocytosis. In the latter case, PP-2 would mimic the Syt11 overexpression phenotype and further inhibit SV endocytosis. When we applied 5 μM PP-2 to WT hippocampal neurons, FM4-64 discharge was inhibited by 11.7% compared with PP-1 (Fig. 7*D*,*F*). Similarly, PP-2 also inhibited the FM4-64 discharge from Syt11-KO terminals by 9.75% (Fig. 7*G*,*I*), partially rescuing the endocytic phenotype. The exocytosis kinetics was unaffected in both experiments, consistent with our KO results (Fig. 7*E*,*H*). In addition, PP-2 decreased the FM4-64 uptake with different durations of electrical stimulation in Syt11-KO terminals (Fig. 7*J*,*K*). When a higher concentration of

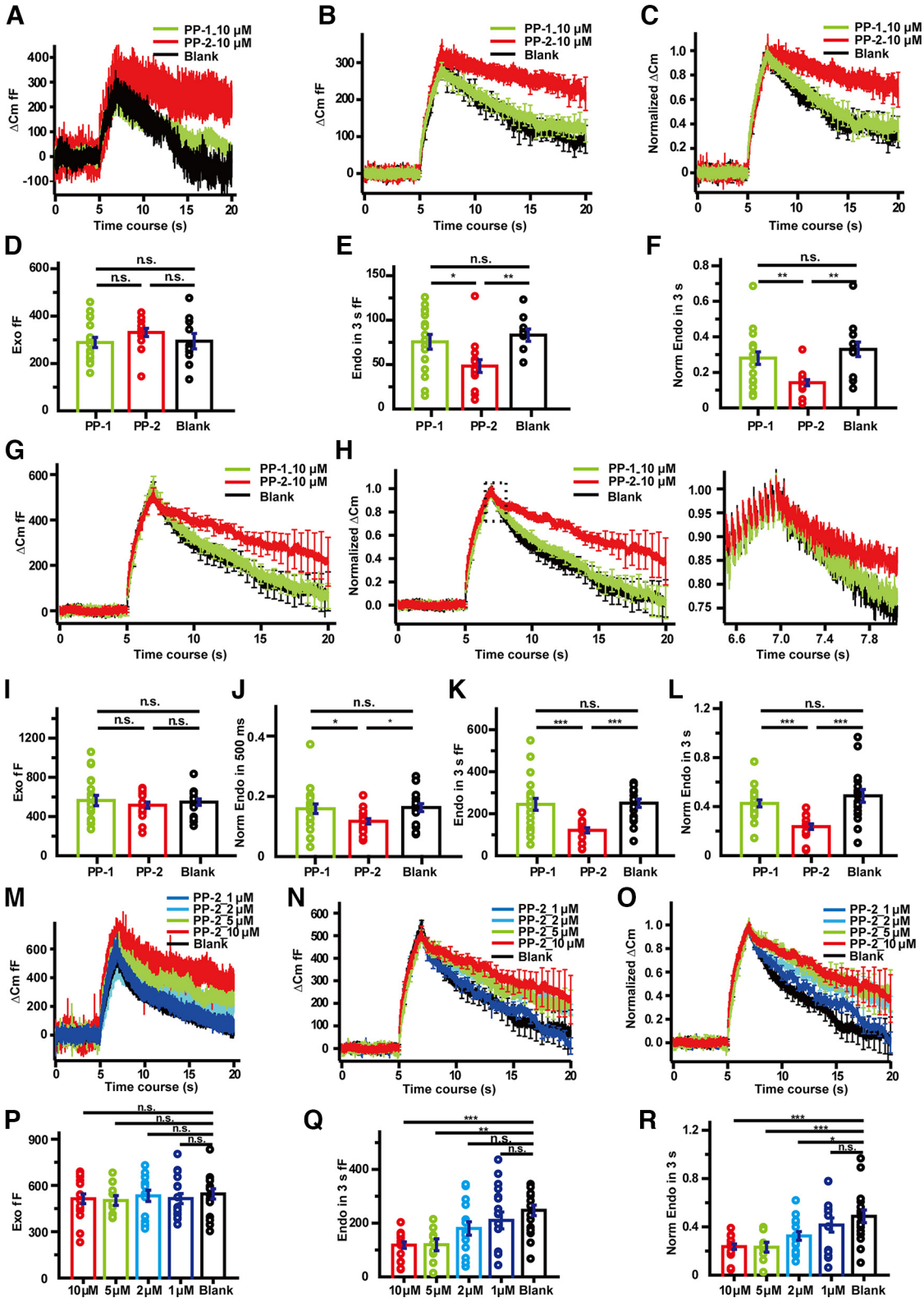

Figure 8. Intracellular application of PP-2 in calyx of Held terminals inhibits the endocytic rate at both room temperature and physiological temperature in a dose-dependent manner. ***A–E***, Example traces (***A***), averaged ΔCm traces (***B***), and averaged normalized ΔCm traces (***C***) in the presence of PP-1 (10 μM, red traces, $n = 17$), PP-2 (10 μM, green traces, $n = 15$), and blank control (black traces, $n = 10$) in the presynaptic pipette at room temperature. The capacitance jump was evoked by 40 AP-e (AP equivalent) at 20 Hz. The SV exocytosis within 2 s (***D***) and endocytosis within the first 3 s after stimulation (***E***, one-way ANOVA: $F = 4.83$, $^{*}p = 0.013$; PP-2 vs PP-1: $^{*}p = 0.016$; PP-2 vs Blank: $^{**}p = 0.007$) were quantified. The normalized endocytic fraction (***F***, one-way ANOVA: $F = 6.57$, $^{**}p = 0.0035$; $^{**}p = 0.002$ for PP-2 vs Blank; $^{**}p = 0.007$ for PP-2 vs PP-1) within first 3 s after stimulation showed significantly decreased endocytosis with PP-2 treatment compared with PP-1, without changing exocytosis (***D***, one-way ANOVA: $F = 0.76$, $p = 0.46$). ***G–L***, Averaged ΔCm traces (***G***) and averaged normalized ΔCm traces (***H***) in the presence of PP-1 (10 μM, red traces, $n = 20$), PP-2 (10 μM, green traces, $n = 17$), and blank control (black traces, $n = 17$) in the presynaptic pipette at physiological temperature. The capacitance jump was evoked by 40 AP-e at 20 Hz. The SV exocytosis within 2 s (***I***) and endocytosis within the first 500 ms (***J***, one-way ANOVA: $F = 3.52$, $^{*}p = 0.037$; PP-2 vs PP-1: $^{*}p = 0.026$; PP-2 vs Blank: $^{*}p = 0.020$) or 3 s after stimulation (***K***, one-way ANOVA: $F = 10.60$, $^{***}p = 0.00014$; PP-2 vs PP-1: $^{***}p = 0.0002$; PP-2 vs Blank: $^{***}p = 0.0002$) were

peptides (25 μM) was applied to WT neurons, the inhibitory effect of PP-2 reached 25.93% compared with PP-1 (Fig. 7*L*,*N*), showing a dose effect. To ensure that the addition of peptides did not affect SV endocytosis nonspecifically, we included a blank control and found that PP-1 application had no effect on SV endocytosis (Fig. 7*L–N*). In addition, PP-2 also inhibited the retrieval of Syt1-pHluorin/Syb2-pHluorin (Fig. 7*O–T*, endocytic τ decreased by 30.19% in Syt1-pHluorin, by 24.74% in Syb2-pHluorin), further supporting the notion that the Syt11–EndoA1 interaction inhibits SV endocytosis.

To investigate the specificity of PP-2 targeting to EndoA1, we applied both PP-1 and PP-2 to EndoA1-KD neurons. Both 5 and 25 μM of peptides were included, and no significant change of FM4-64 discharge was detected compared with blank control in the EndoA1-KD terminals (Fig. 7*U*,*V*). These data demonstrate that PP-2 specifically targets EndoA1 in SV endocytosis. Together, these results support the second scenario of our proposal that Syt11 inhibits EndoA1.

PP-2 peptide dose-dependently inhibits SV endocytosis in the calyx of Held at both room temperature and physiological temperature

To further confirm and quantify the inhibition of endocytosis by this EndoA1-binding peptide, we directly injected PP-1 and PP-2 peptides individually at different concentrations into the presynaptic terminal of the calyx of Held synapse through the whole-cell patch (Sun et al., 2004; Baydyuk et al., 2016). As an assay of exocytosis and endocytosis, capacitance was measured at the calyceal terminals of brain slices containing the median nucleus of the trapezoid body (Paradiso et al., 2007). Exocytosis, as capacitance jumps, was induced by 40 AP-equivalent depolarizing pulses (1 ms, from −80 to 40 mV) at 20 Hz, while the corresponding endocytosis, as the decay of capacitance, was recorded for 20 s after stimulation (Sakaba and Neher, 2001). We first measured the effects of the peptides at room temperature (22°C-24°C) and found that injection of PP-2, but not PP-1, significantly inhibited endocytosis while exocytosis was not affected (Fig. 8*A*,*B*,*D*,*E*). Normalization of capacitance changes to the peak revealed that PP-2 application, compared with PP-1 injection and blank control, caused >30% reduction in membrane retrieval within 3 s after stimulation (Fig. 8*C*,*F*). The inhibition was confirmed not to be because of a mis-targeting effect of the injected peptides because the negative control was the same as the blank control without peptide injection. We obtained the same results at physiological temperature (33°C-35°C). Consistent with a previous report, the induced exocytosis was enhanced and a significant fast component of endocytosis occurred at physiological temperature (Renden and von Gersdorff, 2007; Watanabe et al., 2014) (Fig. 8*G*,*J*). Given that exocytosis was unaffected, application of 10 μM PP-2 significantly inhibited both fast and slow endocytosis, since the membrane retrieval was suppressed by ~40% within 0.5 s and ~50% within 3 s after stimulation compared with the application of PP-1 and blank control (Fig. 8*G*,*J–L*). We further recorded the changes in membrane capacitance induced by 40 AP-equivalent depolarizing pulses after presynaptic injection of various concentrations of PP-2 (1, 2, 5, and 10 μM) at physiological temperature. Correspondingly increasing inhibitory effects on endocytosis occurred with the increasing PP-2 concentration, displaying dose dependence, which tended to saturate at 5 μM (Fig. 8*M–R*). Thus, the Syt11-EndoA1 interaction significantly inhibits SV endocytosis at calyx of Held synapses.

Discussion

Here, we investigated the function of Syt11 in SV endocytosis and the underlying molecular mechanism. Our experiments showed no difference in FM4-64 discharge between WT and Syt11-KO hippocampal synapses under sufficiently prolonged stimulation, while FM4-64 uptake was significantly accelerated (Fig. 1*H–L*). Consistently, a larger fraction of the vesicles in the recycling pool in Syt11-KO than WT synapses were labeled during 60 s of high K^+ stimulation (Fig. 1*E–G*). Moreover, the retrieval of pHluorin-tagged Syt1 and Syb2 from the plasma membrane was faster in Syt11-KO neurons (Fig. 1*M–P*). To observe the phenotype of Syt11 deficiency on neurotransmission as the impact of the change of vesicle recycling, we recorded the eIPSC corresponding to 400 stimuli at different frequencies (10/20 Hz) in primary hippocampal neurons (Fig. 2). Similar to the previous work on cultured cortical neurons (Shimojo et al., 2019), we found no impact of loss of Syt11 on the first 100 AP-evoked transmitter releases at 10 or 20 Hz (Fig. 2*C*,*D*). However, the significant phenotype of Syt11-KO, the enhancement of IPSCs within largely prolonged period (longer than 25 s and 6 s corresponding to 10 Hz and 20 Hz stimuli) could be observed (Fig. 2*E*,*F*). These results suggested that Syt11 loss caused acceleration of endocytosis increases the reused vesicle availability, and no phenotype can be observed before recycled vesicle participation. Our studies confirmed that Syt11 deficiency enhances SV endocytosis without directly affecting exocytosis (Wang et al., 2016, 2018), leaving the molecular mechanism to be elucidated.

The direct involvement of Syt11 in SV endocytosis was strongly suggested as synaptosome fractionation experiments and immunofluorescence analysis revealed the localization of Syt11 at synapses (Fig. 4). Several lines of evidence converge on the conclusion that Syt11 is mainly localized in the plasma membrane of synapses to play its role in SV endocytosis. As reported previously, Syt11 has been shown to regulate the number of endocytic sites during neuronal endocytosis (Wang et al., 2016). This study further showed that endogenous Syt11 was localized in the plasma membrane (B-Δcre, Fig. 3*A*), membrane fractions (F2 and F3, Fig. 4*C*), and synaptosomes (F4, Fig. 4*C*), while myc-Syt11 partially colocalized with endocytic and exocytic proteins (Fig. 4*B*,*D*). Maximov's group (Shimojo et al., 2019) also reported a Syt11 fraction on the axonal plasma membrane and in the low-speed pellets of detergent-free brain homogenates. The partial colocalization of Syt11 with SV proteins probably occurs at the plasma membrane before SV proteins are internalized (Fernandez-Alfonso et al., 2006; Darna et al., 2009; Mutch et al.,

←

quantified. The normalized endocytic fraction (***L***, one-way ANOVA: $F = 12.59$, $^{***}p < 0.001$; PP-2 vs PP-1: $^{***}p = 0.00002$; PP-2 vs Blank: $^{***}p = 0.0004$) within the first 3 s after stimulation showed significantly decreased endocytosis with PP-2 treatment compared with PP-1, without changing exocytosis (***I***, one-way ANOVA: $F = 0.35$, $p = 0.71$). ***M–R***, Example traces (***M***), averaged ΔCm traces (***N***), and averaged normalized ΔCm traces (***O***) in the presence of different concentrations of PP-2 (1 μM, cyan, $n = 17$; 2 μM, red, $n = 15$; 5 μM, blue, $n = 10$; 10 μM, green, $n = 17$) in the presynaptic pipette and blank control (black, $n = 17$) at physiological temperature. The SV exocytosis within 2 s (***P***, one-way ANOVA: $F = 0.25$, $p = 0.91$) and endocytosis within the first 3 s after stimulation were quantified (***Q***, one-way ANOVA: $F = 6.05$, $^{***}p = 0.00030$; 10 μM vs Blank: $^{***}p = 0.0001$; 5 μM vs Blank: $^{**}p = 0.0011$). The normalized endocytic fraction (***R***, one-way ANOVA: $F = 6.19$, $^{***}p = 0.00025$; 10 μM vs Blank: $^{***}p = 0.0009$; 5 μM vs Blank: $^{***}p = 0.0002$; 2 μM vs Blank: $^{*}p = 0.019$) within the first 3 s after stimulation showed that the inhibition by PP-2 was dose-dependent, and saturated at 5 μM. Each group contains at least 8 mice. Data are mean ± SEM. $^{*}p < 0.05$. $^{**}p < 0.01$. $^{***}p < 0.001$.

2011) and Syt11 is not detected in the postendocytic SVs along the recycling pathway (Takamori et al., 2006; Shimojo et al., 2019). We also found Syt1, Syp1, and Syb2 in the plasma membrane together with TfR, Na^+/K^+ ATPase, and SNAP25 (B-cre and B-ΔCre, Fig. 3*A*). The membrane localization of Syt11 is consistent with the finding that the majority of endocytic proteins, including clathrin, endophilin, and amphiphysin, are not found in SVs (Takamori et al., 2006). It is plausible that a fraction of endocytic proteins normally reside at the plasma membrane and function in membrane internalization. Apparently, these proteins are absent from most SVs in terminals. Importantly, our analysis showed tight spatial coupling of Syt11 and EndoA1, which provides further support for the direct interaction between these endocytic proteins.

EndoA1 is highly enriched in the brain and reported to be critical for CME, fast endocytosis in the ribbon synapse, and ultrafast endocytosis (de Heuvel et al., 1997; Chen et al., 2003; Llobet et al., 2011; Zhang et al., 2012; Watanabe et al., 2018). Among the three endophilin A proteins (A1-A3) in the brain, A1 (EndoA1) is the most abundantly expressed and its acute blockade by antibody or KD leads to a range of synaptic defects in SV exocytosis, endocytosis, spine morphogenesis, and stability (Ringstad et al., 1999; Weston et al., 2011; Yang et al., 2015; Zhang et al., 2015a). Moreover, EndoA1 is linked to several brain disorders, such as Alzheimer's disease, Parkinson's disease, epilepsy, and schizophrenia (Ren et al., 2008; Chang et al., 2017; Yu et al., 2018; Corponi et al., 2019). Surprisingly, EndoA1-KO mice appear normal while double or triple KO of endophilin A1-A3 causes severe neurologic defects (Milosevic et al., 2011), suggesting a compensatory effect in the EndoA1-KO mice. Here we found that EndoA1 interacted with Syt11 with high affinity (Fig. 5). The N-terminal BAR domain of EndoA1 self-assembles to form a dimer and stabilizes the high curvature of the plasma membrane (Daumke et al., 2014). On the other hand, the C-terminal SH3 domain interacts with endocytic players in vesicle fission and clathrin uncoating (Gad et al., 2000; Verstreken et al., 2003; Milosevic et al., 2011; Pechstein et al., 2015; Cao et al., 2017). As EndoA1 plays roles in membrane sculpting (Cui et al., 2009; Suresh and Edwardson, 2010; Mim et al., 2012; McMahon and Boucrot, 2015; Poudel et al., 2016; Simunovic et al., 2017), vesicle fission (Daumke et al., 2014), and clathrin uncoating (Gad et al., 2000; Verstreken et al., 2003; Milosevic et al., 2011), we proposed that Syt11 inhibits SV endocytosis mainly through direct interaction with EndoA1. In support, we found that Syt11 was in the same immunocomplex as EndoA1 in brain extracts and they directly interacted in a Ca^{2+}-independent manner (Fig. 5*A–G*), while Syt11 did not affect EndoA1 expression in synapses (Fig. 5*E*). We also mapped the binding sequences in both Syt11 and EndoA1 proteins and found that Syt11 bound the N-terminal of EndoA1, not the SH3 domain which recruits dynamin and synaptojanin. The binding site in Syt11 was mapped to an amino acid sequence in its C2B domain (a.a. 314-336, PP-2). We then used the strategy of direct application of the peptides into terminals. The peptide experiments had two advantages. First, this amino acid stretch of Syt11 was found to be specific for EndoA1 targeting (it has no effect on EndoA1-KD neurons) and thus led us to investigate the function of the Syt11–EndoA1 interaction. Second, acute peptide treatment circumvents the potential compensatory effects in KD or KO experiments.

In our study, inhibition of SV endocytosis by PP-2 was observed not only in high K^+ stimulation-induced endocytosis on hippocampal synapses at room temperature but also in 40 AP-equivalent depolarizing pulses induced endocytosis in calyx of Held synapses at physiological temperature (Fig. 8) (Granseth et al., 2006; Watanabe et al., 2013; Delvendahl et al., 2016). In hippocampal neuron terminals with mostly small synapses, endocytic pathways include CME (Granseth et al., 2006) and bulk endocytosis (Clayton and Cousin, 2009). At the calyx of Held synapse, which is a giant glutamatergic synapse, endocytic pathways may include a slow component because of CME and bulk endocytosis, and a fast, possibly clathrin-independent, endocytosis (Gan and Watanabe, 2018). Our experiments on the calyx of Held were performed at physiological temperature on immature mice (P8-P10) when both fast and slow endocytosis can be recorded, and both were affected by intraterminal peptide application (Fig. 8*G–L*) (Smith et al., 2008; Yamashita et al., 2010; Watanabe et al., 2013). During maturation, synapses of the calyx of Held undergo a developmental shift and different mechanisms of fast and slow endocytosis are involved, including nanodomain Ca^{2+} as well as calmodulin and calcineurin independence (Hosoi et al., 2009; Wu et al., 2009; Yamashita et al., 2010). As we found that the Syt11-EndoA1 interaction was Ca^{2+}-independent (Fig. 5*G*), we suggest that this interaction also regulates both forms of endocytosis in mature synapses. Future studies are needed to answer this question. EndoA1 is required for multiple modes of endocytosis (de Heuvel et al., 1997; Chen et al., 2003; Llobet et al., 2011; Zhang et al., 2012; Boucrot et al., 2015; Watanabe et al., 2018). The fact that peptide application reduced SV endocytosis at both types of synapse and partially rescued the phenotype in Syt11-KO hippocampal neurons, mimicking the action of Syt11 as a down-regulator of EndoA1 activity, supports the conclusion that Syt11 inhibits EndoA1 function in different modes of SV endocytosis.

To investigate the impact of Syt11 on regulating membrane protein retrieval, we examined the synaptic protein partition at the plasma membrane. We found abnormal partition of TfR and Syt1 while Syb2, Syp1, and SNAP25 were unaffected in Syt11-KO neurons. These results show that Syt11 regulates the retrieval fidelity of selective synaptic proteins. Interestingly, Mutch et al. (2011) reported that a subset of SV proteins, including Syt1, SV2, the proton ATPase, and Vglut1, are sorted to vesicles with high precision, whereas other proteins, such as Syb2, Syp1, and synaptogyrin, have a large variation in the numbers in single vesicles. Our data suggest that Syt11 regulates the targeting synaptic proteins that undergo high-precision retrieval. It is possible that these two classes of synaptic proteins have different internalization mechanisms and the high-precision proteins undergo relatively sophisticated sorting and checkpoint processes, which are more time-consuming. In the absence of Syt11, SV endocytosis accelerates and the high-precision proteins fail to be retrieved properly. TfR and Syt1 both undergo CME. TfR is distributed all over the neuronal surface, including the synapse, and is internalized constitutively (Rosendale et al., 2017). The increased level of TfR on the plasma membrane could also contribute to the enhanced Tf uptake previously reported in Syt11-KD and -KO neurons (Wang et al., 2016, 2018). On the other hand, Syt1 is highly enriched in neuronal synapses, and we found decreased membrane partition of Syt1 in Syt11-KO synapses. Syt1 retrieval is known to involve AP2 (Zhang et al., 1994), stonin 2 (Kononenko et al., 2013; Kaempf et al., 2015), and SV2 (Yao et al., 2010; Zhang et al., 2015b). The protein partition at synaptic membrane is largely determined by synaptic activity (Koo et al., 2011; Kononenko et al., 2013). As Syt11 did not affect evoked exocytosis, the reduced Syt1 partition in Syt11-KO synapses was most likely caused by increased endocytosis. Therefore, we reason that Syt11 safeguards the high-precision synaptic protein retrieval by preventing the hyperactivity of

SV endocytosis, helping to ensure the accurate recruitment/enrichment of endocytic cargoes at endocytic sites.

To date, a few proteins have been proposed to safeguard the precision of specific synaptic protein retrieval during SV endocytosis (Gordon and Cousin, 2016), such as AP180/CALM for Syb2 (Koo et al., 2011, 2015), stonin 2 and SV2 for Syt1 (Yao et al., 2010; Kononenko et al., 2013; Kaempf et al., 2015; Zhang et al., 2015b), and Syb2 for Syp (Gordon et al., 2011). A recent study also reported Hsc70 as a checkpoint protein for cargo incorporation during CME using a cell-free reconstitution system (Chen et al., 2019). Here, we propose a novel mechanism for precise synaptic protein homeostasis during SV endocytosis. Syt11 downregulates SV endocytosis via interaction with EndoA1 to ensure precise cargo recruitment at the expense of endocytic rate. As both Syt11 and EndoA1 are associated with Parkinson's disease and schizophrenia, this regulation may play important roles under physiological and pathologic conditions.

References

Anggono V, Robinson PJ (2007) Syndapin I and endophilin I bind overlapping proline-rich regions of dynamin I: role in synaptic vesicle endocytosis. J Neurochem 102:931–943.

Baydyuk M, Xu J, Wu LG (2016) The calyx of Held in the auditory system: structure, function, and development. Hear Res 338:22–31.

Bento CF, Ashkenazi A, Jimenez-Sanchez M, Rubinsztein DC (2016) The Parkinson's disease-associated genes ATP13A2 and SYT11 regulate autophagy via a common pathway. Nat Commun 7:11803.

Betz WJ, Bewick GS (1992) Optical analysis of synaptic vesicle recycling at the frog neuromuscular junction. Science 255:200–203.

Boucrot E, et al. (2015) Endophilin marks and controls a clathrin-independent endocytic pathway. Nature 517:460–465.

Cao M, Wu Y, Ashrafi G, McCartney AJ, Wheeler H, Bushong EA, Boassa D, Ellisman MH, Ryan TA, De Camilli P (2017) Parkinson sac domain mutation in synaptojanin 1 impairs clathrin uncoating at synapses and triggers dystrophic changes in dopaminergic axons. Neuron 93:882–896. e5.

Chang D, et al. (2017) A meta-analysis of genome-wide association studies identifies 17 new Parkinson's disease risk loci. Nat Genet 49: 1511–1516.

Chen Y, Deng L, Maeno-Hikichi Y, Lai M, Chang S, Chen G, Zhang JF (2003) Formation of an endophilin-Ca^{2+} channel complex is critical for clathrin-mediated synaptic vesicle endocytosis. Cell 115:37–48.

Chen Y, Yong J, Martinez-Sanchez A, Yang Y, Wu Y, De Camilli P, Fernandez-Busnadiego R, Wu M (2019) Dynamic instability of clathrin assembly provides proofreading control for endocytosis. J Cell Biol 218:3200–3211.

Clayton EL, Cousin MA (2009) The molecular physiology of activity-dependent bulk endocytosis of synaptic vesicles. J Neurochem 111:901–914.

Corponi F, Bonassi S, Vieta E, Albani D, Frustaci A, Ducci G, Landi S, Boccia S, Serretti A, Fabbri C (2019) Genetic basis of psychopathological dimensions shared between schizophrenia and bipolar disorder. Prog Neuropsychopharmacol Biol Psychiatry 89:23–29.

Cui H, Ayton GS, Voth GA (2009) Membrane binding by the endophilin N-BAR domain. Biophys J 97:2746–2753.

Daumke O, Roux A, Haucke V (2014) BAR domain scaffolds in dynamin-mediated membrane fission. Cell 156:882–892.

Darna M, Schmutz I, Richter K, Yelamanchili SV, Pendyala G, Holtje M, Albrecht U, Ahnert-Hilger G (2009) Time of day-dependent sorting of the vesicular glutamate transporter to the plasma membrane. J Biol Chem 284:4300–4307.

de Heuvel E, Bell AW, Ramjaun AR, Wong K, Sossin WS, McPherson PS (1997) Identification of the major synaptojanin-binding proteins in brain. J Biol Chem 272:8710–8716.

Deak F, Schoch S, Liu X, Sudhof TC, Kavalali ET (2004) Synaptobrevin is essential for fast synaptic-vesicle endocytosis. Nat Cell Biol 6:1102–1108.

Delvendahl I, Vyleta NP, von Gersdorff H, Hallermann S (2016) Fast, temperature-sensitive and clathrin-independent endocytosis at central synapses. Neuron 90:492–498.

Diao J, Cipriano DJ, Zhao M, Zhang Y, Shah S, Padolina MS, Pfuetzner RA, Brunger AT (2013) Complexin-1 enhances the on-rate of vesicle docking via simultaneous SNARE and membrane interactions. J Am Chem Soc 135:15274–15277.

Dunkley PR, Jarvie PE, Robinson PJ (2008) A rapid Percoll gradient procedure for preparation of synaptosomes. Nat Protoc 3:1718–1728.

Fernandez-Alfonso T, Kwan R, Ryan TA (2006) Synaptic vesicles interchange their membrane proteins with a large surface reservoir during recycling. Neuron 51:179–186.

Gad H, Ringstad N, Löw P, Kjaerulff O, Gustafsson J, Wenk M, Di Paolo G, Nemoto Y, Crun J, Ellisman MH, De Camilli P, Shupliakov O, Brodin L (2000) Fission and uncoating of synaptic clathrin-coated vesicles are perturbed by disruption of interactions with the SH3 domain of endophilin. Neuron 27:301–312.

Gan Q, Watanabe S (2018) Synaptic vesicle endocytosis in different model systems. Front Cell Neurosci 12:171.

Glass AS, Huynh DP, Franck T, Woitalla D, Muller T, Pulst SM, Berg D, Kruger R, Riess O (2004) Screening for mutations in synaptotagmin XI in Parkinson's disease. J Neural Transm Suppl 21–28.

Gordon SL, Cousin MA (2016) The iTRAPs: guardians of synaptic vesicle cargo retrieval during endocytosis. Front Synaptic Neurosci 8:1.

Gordon SL, Leube RE, Cousin MA (2011) Synaptophysin is required for synaptobrevin retrieval during synaptic vesicle endocytosis. J Neurosci 31:14032–14036.

Granseth B, Odermatt B, Royle SJ, Lagnado L (2006) Clathrin-mediated endocytosis is the dominant mechanism of vesicle retrieval at hippocampal synapses. Neuron 51:773–786.

Hosoi N, Holt M, Sakaba T (2009) Calcium dependence of exo- and endocytotic coupling at a glutamatergic synapse. Neuron 63:216–229.

Huynh DP, Scoles DR, Nguyen D, Pulst SM (2003) The autosomal recessive juvenile Parkinson disease gene product, parkin, interacts with and ubiquitinates synaptotagmin XI. Hum Mol Genet 12:2587–2597.

Inoue S, Imamura A, Okazaki Y, Yokota H, Arai M, Hayashi N, Furukawa A, Itokawa M, Oishi M (2007) Synaptotagmin XI as a candidate gene for susceptibility to schizophrenia. Am J Med Genet B Neuropsychiatr Genet 144B:332–340.

Iwabuchi S, Kakazu Y, Koh JY, Goodman KM, Harata NC (2014) Examination of synaptic vesicle recycling using FM4-64 dyes during evoked, spontaneous, and miniature synaptic activities. J Vis Exp 50557.

Kaempf N, Kochlamazashvili G, Puchkov D, Maritzen T, Bajjalieh SM, Kononenko NL, Haucke V (2015) Overlapping functions of stonin 2 and SV2 in sorting of the calcium sensor synaptotagmin 1 to synaptic vesicles. Proc Natl Acad Sci USA 112:7297–7302.

Kononenko NL, Diril MK, Puchkov D, Kintscher M, Koo SJ, Pfuhl G, Winter Y, Wienisch M, Klingauf J, Breustedt J (2013) Compromised fidelity of endocytic synaptic vesicle protein sorting in the absence of stonin 2. Proc Natl Acad Sci USA 110:E526–E535.

Koo SJ, et al. (2015) Vesicular synaptobrevin/VAMP2 levels guarded by AP180 control efficient neurotransmission. Neuron 88:330–344.

Koo SJ, Markovic S, Puchkov D, Mahrenholz CC, Beceren-Braun F, Maritzen T, Dernedde J, Volkmer R, Oschkinat H, Haucke V (2011) SNARE motif-mediated sorting of synaptobrevin by the endocytic adaptors clathrin assembly lymphoid myeloid leukemia (CALM) and AP180 at synapses. Proc Natl Acad Sci USA 108:13540–13545.

Leitz J, Kavalali ET (2016) Ca^{2+} dependence of synaptic vesicle endocytosis. Neuroscientist 22:464–476.

Li YC, Chanaday NL, Xu W, Kavalali ET (2017) Synaptotagmin-1- and synaptotagmin-7-dependent fusion mechanisms target synaptic vesicles to kinetically distinct endocytic pathways. Neuron 93:616–631. e3.

Li Z, Burrone J, Tyler WJ, Hartman KN, Albeanu DF, Murthy VN (2005) Synaptic vesicle recycling studied in transgenic mice expressing synaptopHluorin. Proc Natl Acad Sci USA 102:6131–6136.

Llobet A, Gallop JL, Burden JJ, Camdere G, Chandra P, Vallis Y, Hopkins CR, Lagnado L, McMahon HT (2011) Endophilin drives the fast mode of vesicle retrieval in a ribbon synapse. J Neurosci 31:8512–8519.

Lou X (2018) Sensing exocytosis and triggering endocytosis at synapses: synaptic vesicle exocytosis-endocytosis coupling. Front Cell Neurosci 12:66.

McMahon HT, Boucrot E (2015) Membrane curvature at a glance. J Cell Sci 128:1065–1070.

Micheva KD, Kay BK, McPherson PS (1997a) Synaptojanin forms two separate complexes in the nerve terminal: interactions with endophilin and amphiphysin. J Biol Chem 272:27239–27245.

Micheva KD, Ramjaun AR, Kay BK, McPherson PS (1997b) SH3 domain-dependent interactions of endophilin with amphiphysin. FEBS Lett 414:308–312.

Miesenbock G, De Angelis DA, Rothman JE (1998) Visualizing secretion and synaptic transmission with pH-sensitive green fluorescent proteins. Nature 394:192–195.

Milosevic I (2018) Revisiting the role of clathrin-mediated endoytosis in synaptic vesicle recycling. Front Cell Neurosci 12:27.

Milosevic I, et al. (2011) Recruitment of endophilin to clathrin-coated pit necks is required for efficient vesicle uncoating after fission. Neuron 72:587–601.

Mim C, Cui H, Gawronski-Salerno JA, Frost A, Lyman E, Voth GA, Unger VM (2012) Structural basis of membrane bending by the N-BAR protein endophilin. Cell 149:137–145.

Mittelsteadt T, Seifert G, Alvarez-Baron E, Steinhauser C, Becker AJ, Schoch S (2009) Differential mRNA expression patterns of the synaptotagmin gene family in the rodent brain. J Comp Neurol 512:514–528.

Mutch SA, et al. (2011) Protein quantification at the single vesicle level reveals that a subset of synaptic vesicle proteins are trafficked with high precision. J Neurosci 31:1461–1470.

Paradiso K, Wu W, Wu LG (2007) Methods for patch clamp capacitance recordings from the calyx. J Vis Exp 244.

Pechstein A, et al. (2015) Vesicle uncoating regulated by SH3-SH3 domain-mediated complex formation between endophilin and intersectin at synapses. EMBO Rep 16:232–239.

Pihlstrom L, et al. (2013) Supportive evidence for 11 loci from genome-wide association studies in Parkinson's disease. Neurobiol Aging 34:1708.

Poskanzer KE, Marek KW, Sweeney ST, Davis GW (2003) Synaptotagmin I is necessary for compensatory synaptic vesicle endocytosis in vivo. Nature 426:559–563.

Poudel KR, Dong Y, Yu H, Su A, Ho T, Liu Y, Schulten K, Bai J (2016) A time course of orchestrated endophilin action in sensing, bending, and stabilizing curved membranes. Mol Biol Cell 27:2119–2132.

Qiu X, Zhu Q, Sun J (2015) Quantitative analysis of vesicle recycling at the calyx of Held synapse. Proc Natl Acad Sci USA 112:4779–4784.

Ren Y, et al. (2008) Endophilin I expression is increased in the brains of Alzheimer disease patients. J Biol Chem 283:5685–5691.

Renden R, von Gersdorff H (2007) Synaptic vesicle endocytosis at a CNS nerve terminal: faster kinetics at physiological temperatures and increased endocytotic capacity during maturation. J Neurophysiol 98:3349–3359.

Ringstad N, Gad H, Low P, Di Paolo G, Brodin L, Shupliakov O, De Camilli P (1999) Endophilin/SH3p4 is required for the transition from early to late stages in clathrin-mediated synaptic vesicle endocytosis. Neuron 24:143–154.

Ringstad N, Nemoto Y, De Camilli P (1997) The SH3p4/Sh3p8/SH3p13 protein family: binding partners for synaptojanin and dynamin via a Grb2-like Src homology 3 domain. Proc Natl Acad Sci USA 94:8569–8574.

Rosendale M, Jullie D, Choquet D, Perrais D (2017) Spatial and temporal regulation of receptor endocytosis in neuronal dendrites revealed by imaging of single vesicle formation. Cell Rep 18:1840–1847.

Saheki Y, De Camilli P (2012) Synaptic vesicle endocytosis. Cold Spring Harb Perspect Biol 4:a005645.

Sakaba T, Neher E (2001) Calmodulin mediates rapid recruitment of fast-releasing synaptic vesicles at a calyx-type synapse. Neuron 32:1119–1131.

Schivell AE, Batchelor RH, Bajjalieh SM (1996) Isoform-specific, calcium-regulated interaction of the synaptic vesicle proteins SV2 and synaptotagmin. J Biol Chem 271:27770–27775.

Sesar A, et al. (2016) Synaptotagmin XI in Parkinson's disease: new evidence from an association study in Spain and Mexico. J Neurol Sci 362:321–325.

Shimizu H, Kawamura S, Ozaki K (2003) An essential role of Rab5 in uniformity of synaptic vesicle size. J Cell Sci 116:3583–3590.

Shimojo M, Madara J, Pankow S, Liu X, Yates J 3rd, Sudhof TC, Maximov A (2019) Synaptotagmin-11 mediates a vesicle trafficking pathway that is essential for development and synaptic plasticity. Genes Dev 33:365–376.

Simunovic M, et al. (2017) Friction mediates scission of tubular membranes scaffolded by BAR proteins. Cell 170:172–184. e11.

Smith SM, Renden R, von Gersdorff H (2008) Synaptic vesicle endocytosis: fast and slow modes of membrane retrieval. Trends Neurosci 31:559–568.

Soykan T, Maritzen T, Haucke V (2016) Modes and mechanisms of synaptic vesicle recycling. Curr Opin Neurobiol 39:17–23.

Sun JY, Wu XS, Wu W, Jin SX, Dondzillo A, Wu LG (2004) Capacitance measurements at the calyx of Held in the medial nucleus of the trapezoid body. J Neurosci Methods 134:121–131.

Sundborger A, Soderblom C, Vorontsova O, Evergren E, Hinshaw JE, Shupliakov O (2011) An endophilin-dynamin complex promotes budding of clathrin-coated vesicles during synaptic vesicle recycling. J Cell Sci 124:133–143.

Suresh S, Edwardson JM (2010) The endophilin N-BAR domain perturbs the structure of lipid bilayers. Biochemistry 49:5766–5771.

Takamori S, et al. (2006) Molecular anatomy of a trafficking organelle. Cell 127:831–846.

Verstreken P, Koh TW, Schulze KL, Zhai RG, Hiesinger PR, Zhou Y, Mehta SQ, Cao Y, Roos J, Bellen HJ (2003) Synaptojanin is recruited by endophilin to promote synaptic vesicle uncoating. Neuron 40:733–748.

Verstreken P, Ohyama T, Bellen HJ (2008) FM1-43 labeling of synaptic vesicle pools at the *Drosophila* neuromuscular junction. Methods Mol Biol 440:349–369.

Vinatier J, Herzog E, Plamont MA, Wojcik SM, Schmidt A, Brose N, Daviet L, El Mestikawy S, Giros B (2006) Interaction between the vesicular glutamate transporter type 1 and endophilin A1, a protein essential for endocytosis. J Neurochem 97:1111–1125.

von Poser C, Ichtchenko K, Shao X, Rizo J, Sudhof TC (1997) The evolutionary pressure to inactivate: a subclass of synaptotagmins with an amino acid substitution that abolishes Ca^{2+} binding. J Biol Chem 272:14314–14319.

Wang C, Wang Y, Hu M, Chai Z, Wu Q, Huang R, Han W, Zhang CX, Zhou Z (2016) Synaptotagmin-11 inhibits clathrin-mediated and bulk endocytosis. EMBO Rep 17:47–63.

Wang C, et al. (2018) Synaptotagmin-11 is a critical mediator of parkin-linked neurotoxicity and Parkinson's disease-like pathology. Nat Commun 9:81.

Wang YL, Zhang CX (2017) Putting a brake on synaptic vesicle endocytosis. Cell Mol Life Sci 74:2917–2927.

Watanabe S, Boucrot E (2017) Fast and ultrafast endocytosis. Curr Opin Cell Biol 47:64–71.

Watanabe S, Rost BR, Camacho-Perez M, Davis MW, Sohl-Kielczynski B, Rosenmund C, Jorgensen EM (2013) Ultrafast endocytosis at mouse hippocampal synapses. Nature 504:242–247.

Watanabe S, Trimbuch T, Camacho-Perez M, Rost BR, Brokowski B, Sohl-Kielczynski B, Felies A, Davis MW, Rosenmund C, Jorgensen EM (2014) Clathrin regenerates synaptic vesicles from endosomes. Nature 515:228–233.

Watanabe S, et al. (2018) Synaptojanin and endophilin mediate neck formation during ultrafast endocytosis. Neuron 98:1184–1197. e6.

Weston MC, Nehring RB, Wojcik SM, Rosenmund C (2011) Interplay between VGLUT isoforms and endophilin A1 regulates neurotransmitter release and short-term plasticity. Neuron 69:1147–1159.

Wu LG, Hamid E, Shin W, Chiang HC (2014) Exocytosis and endocytosis: modes, functions, and coupling mechanisms. Annu Rev Physiol 76:301–331.

Wu XS, McNeil BD, Xu J, Fan J, Xue L, Melicoff E, Adachi R, Bai L, Wu LG (2009) Ca^{2+} and calmodulin initiate all forms of endocytosis during depolarization at a nerve terminal. Nat Neurosci 12:1003–1010.

Wu XS, Zhang Z, Zhao WD, Wang D, Luo F, Wu LG (2014) Calcineurin is universally involved in vesicle endocytosis at neuronal and nonneuronal secretory cells. Cell Rep 7:982–988.

Xu J, Luo F, Zhang Z, Xue L, Wu XS, Chiang HC, Shin W, Wu LG (2013) SNARE proteins synaptobrevin, SNAP-25, and syntaxin are involved in rapid and slow endocytosis at synapses. Cell Rep 3:1414–1421.

Yamashita T, Eguchi K, Saitoh N, von Gersdorff H, Takahashi T (2010) Developmental shift to a mechanism of synaptic vesicle endocytosis requiring nanodomain Ca^{2+}. Nat Neurosci 13:838–844.

Yamashita T (2012) Ca^{2+}-dependent regulation of synaptic vesicle endocytosis. Neurosci Res 73:1–7.

Yang Y, Wei M, Xiong Y, Du X, Zhu S, Yang L, Zhang C, Liu JJ (2015) Endophilin A1 regulates dendritic spine morphogenesis and stability through interaction with p140Cap. Cell Res 25:496–516.

Yao CK, Lin YQ, Ly CV, Ohyama T, Haueter CM, Moiseenkova-Bell VY, Wensel TG, Bellen HJ (2009) A synaptic vesicle-associated Ca^{2+} channel

promotes endocytosis and couples exocytosis to endocytosis. Cell 138: 947–960.

Yao J, Nowack A, Kensel-Hammes P, Gardner RG, Bajjalieh SM (2010) Cotrafficking of SV2 and synaptotagmin at the synapse. J Neurosci 30:5569–5578.

Yao LH, Rao Y, Varga K, Wang CY, Xiao P, Lindau M, Gong LW (2012) Synaptotagmin 1 is necessary for the Ca^{2+} dependence of clathrin-mediated endocytosis. J Neurosci 32:3778–3785.

Yu X, Xu T, Ou S, Yuan J, Deng J, Li R, Yang J, Liu X, Li Q, Chen Y (2018) Endophilin A1 mediates seizure activity via regulation of AMPARs in a PTZ-kindled epileptic mouse model. Exp Neurol 304:41–57.

Zhang B, Koh YH, Beckstead RB, Budnik V, Ganetzky B, Bellen HJ (1998) Synaptic vesicle size and number are regulated by a clathrin adaptor protein required for endocytosis. Neuron 21:1465–1475.

Zhang J, Fan J, Tian Q, Song Z, Zhang JF, Chen Y (2012) Characterization of two distinct modes of endophilin in clathrin-mediated endocytosis. Cell Signal 24:2043–2050.

Zhang J, Tan M, Yin Y, Ren B, Jiang N, Guo G, Chen Y (2015a) Distinct functions of endophilin isoforms in synaptic vesicle endocytosis. Neural Plast 2015:371496.

Zhang N, et al. (2015b) Phosphorylation of synaptic vesicle protein 2A at Thr84 by casein kinase 1 family kinases controls the specific retrieval of synaptotagmin-1. J Neurosci 35:2492–2507.

Zhang JZ, Davletov BA, Sudhof TC, Anderson RG (1994) Synaptotagmin I is a high affinity receptor for clathrin AP-2: implications for membrane recycling. Cell 78:751–760.

Zhu Y, Xu J, Heinemann SF (2009) Two pathways of synaptic vesicle retrieval revealed by single-vesicle imaging. Neuron 61:397–411.